PROCEEDINGS
OF THE
NINETY EIGHTH SESSION OF THE
# INDIAN SCIENCE CONGRESS

CHENNAI, 2011

PART II

SECTION OF MATERIALS SCIENCE

*President :* Prof. Samit Kumar Ray

## CONTENTS

# 98th Indian Science Congress

**January 3-7, 2011, Chennai**

# I

# PRESIDENTIAL ADDRESS

*President*

**Prof. Samit K. Ray**

# SILICON GERMANIUM NANOSTRUCTURES FOR ELECTRONIC AND PHOTONIC DEVICES

*President :* **Samit Kumar Ray***

## SECTION OF MATERIALS SCIENCE

## Abstract

Semiconductor nanostructures are attractive because of their potentials in substantial improvements in optical and electrical properties over those of conventional two-dimensional structures. Epitaxial growth of SiGe/Si films in the Stranski-Krastanov mode can be exploited for the self-assembled growth of three-dimensional islands. Synthesis of Si and Ge nanocrystals embedded in a high bandgap insulator matrix could be utilized to achieve nanometer range structures without sophisticated nanolithography techniques. Silicon and germanium nanocrystals are promising candidates for light emission in the visible wavelength range due to quantum confinement of carriers and for flash electrically erasable and programmable read-only memory devices because of the Coulomb blockade phenomena. The author and his group have made a sustained effort over a decade to develop novel group-IV semiconductor nanostructures for applications in next generation electronic and photonic devices. The growth of self-assembled Ge nanostructures by molecular beam epitaxy, light emission in the visible range due to quantum confinement and the charge storage characteristics of Ge nanocrystals embedded in $SiO_2$ matrix are presented. SiGe/Si-based multi-quantum well and quantum dot semiconductor heterostructures are attractive for use in mid-infrared and THz devices because of the compatibility with planar integration technology and the absence of the reststrahlen absorption band that is present in III-V and II-VI compound semiconductors. The results of Ge based quantum dot infrared photodetector working at room temperature are discussed. The optical and electrical properties of one dimensional Ge nanostructures, Ge/CdS core-shell radial heterostructures and Er-doped

---

*Department of Physics and Meteorology, Indian Institute of Technology Kharagpur-721 302, India.*
*E-mail : physkr@phy.iitkgp.ernet.in*

Ge emitting in the fiber optic wavelength range are presented. Memory devices fabricated with metal nanocrystals in Si based MOSFET technology are considered to be attractive for their higher density of states around the Fermi level, a wide range of available work function, stronger coupling with conduction channel and smaller energy perturbation due to carrier confinement. Our recent results on Ni-nanocrystal based floating gate structures for new generation nonvolatile memory devices are reviewed.

## 1. Introduction

The study of semiconductor nanocrystals and quantum dots is an attractive field of research because of their potential applications in novel electronic & optoelectronic devices. With suitable combinations of characteristic length scales in vertical and lateral directions, quantum-mechanical confinement in one, two or three dimension has been possible in a wide variety of structures with quantized energy levels for conduction electrons and holes. Using these quantum-confined structures, novel electronic and photonic devices with unique but tailored properties have become feasible. The carrier confinement in quantum dots or nanocrystals modifies the optical characteristics of the material resulting in superior properties to those of bulk for device applications. In particular, Si based nanostructures received considerable attention for their possible use in optoelectronic applications. Silicon microphotonics, a technology that combines photonics and silicon microelectronic components has rapidly evolved. Bulk crystalline group-IV semiconductors viz., Si and Ge exhibit very weak luminescence due to the indirect bandgap in their electronic structures. Therefore Si and Ge have not been useful materials for the manufacturing of active optical devices. So, the main challenge of silicon photonics is to develop efficient light source using silicon based materials. The observation of strong visible photoluminescence from nano-porous silicon at room temperature in 1990 stimulated substantial activity in the field of preparation of such structures as well as exploration of their optoelectronic properties. Later, intense visible photoluminescence was reported from nanocrystalline silicon films and $SiO_2$ thin films containing crystalline or amorphous silicon nanoparticles. The emission wavelength due to radiative recombination of carriers could be suitably modified by changing the nanocrystal size.

The growth of Ge islands on Si substrates via Stranski–Krastanov growth mode has been extensively investigated as this opens up the possibility to integrate optoelectronics with planar Si technology [1-3]. Most of the SiGe/Si structures are believed to exhibit a type-II heterointerface, where electrons and holes are spatially separated with a limited wave function overlap. Owing

to the type-II band alignment, Ge quantum dots (QDs) themselves form a potential well only for holes, whereas the electrons are weakly confined in their vicinity, i.e., by the tensile and compressive strain fields in the Si cap induced by the strained QDs. This has led to the enhancement of photoluminescence (PL) quantum efficiency in planar Si/SiGe superlattices at elevated temperatures due to 3D carrier localization within the Ge QDs and presumably due to large energy barriers formed at the heterointerfaces between the Ge clusters and the surrounding Si matrix.

On the other hand, intersubband transitions in Ge/Si quantum dots are attractive for quantum dot infrared photodetectors (QDIPs) in the wavelength range 5-10 $\mu$m. Ge QDIPs have an advantage that the absorption of normally incident infrared radiation by holes in the valence band is allowed, without the requirement of fabrication of gratings or any other optical coupling elements unlike for the conduction band of III-V semiconductors. Similarly, persistent efforts have been made to achieve efficient visible light emission from Si and Ge nanocrystals (NCs) embedded in oxide matrix. Even though Ge NCs embedded in the high band gap oxide matrix show efficient and tunable PL emission by varying their size, the origin of the light emission is still under debate. Er-implanted $SiO_2$ films have recently attracted considerable interest due to the possibility of making light emitting devices that operate at a wavelength of 1.54 $\mu$m [4-5]. The devices are fully compatible with Si-based integrated circuit (IC) technology, thus permitting their integration into advanced Si ICs. Low emission efficiencies observed in bulk indirect gap Si can be overcome by charge trapping in Er doped $SiO_2$ containing Si or Ge nanocrystals.

Semiconductor heterojunctions grown on one dimensional nanowire templates have been demonstrated to be useful for photo-electrochemical cell [6], light-emitting diodes [7], electro-chromic devices [8] and sensor systems [9]. The core-shell nanowire heterojunction possesses a unique advantage of high surface area-to-volume ratio with carrier separation taking place in the junction in radial direction within one diffusion length of minority carriers. CdS is an important direct band gap semiconductor with strong optical absorption in the visible range but exhibits only n-type behavior due to compensation effects. Ge/CdS core-shell nanowire radial heterostructures have been found to be extremely useful for broadband optoelectronic devices such as photodetectors and solar cells with photoresponse covering visible to near-IR regions.

Non-volatile floating-gate flash memories (NVFM) based on charge storage in discrete semiconductor and metal nanocrystals (NCs) have generated increasing interest for their advantages like low operating power, faster access time, larger retention, cycling, and scalability

over traditional flash EEPROMs and their large variety of applications in modern microprocessor-based devices [10, 11]. Nanocrystals acting as floating gates, embedded between the blocking and tunneling oxide, can significantly improve the non-volatile charge retention time due to the effects of Coulomb blockade, quantum confinement, and reduction of charge leakage from weak spots in the tunnel oxide. Most of the studies including ours have focused on the fabrication of metal–oxide-semiconductor (MOS) structures having semiconductor NCs. Nevertheless, The use of metal-NCs is more preferable for its possibility to be used at small operating voltages, better cycling and faster write/erase speeds with smaller fluctuations and interface states.

In view of the above, the present review will highlight the recent contributions and achievements in the research group of the present author with regards to the development of group-IV semiconductor based nanostructures for possible applications in next generation electronic and photonic devices. The overall scope and objectives of the study and review are:

- Growth of self assembled Ge quantum dots on Si (100) and embedded in oxide matrices.

- Electrical and optical properties of Ge nanocrystal based light emitters and floating gate memory devices

- Investigation on Er-doped Ge nanowires for light emitting devices that operates at a wavelength of 1.54 $\mu$m.

- Fabrication of Ge/CdS radial nanowire heterostructures for broadband optical devices

- Investigation on Ni nanocrystal based Si MOS structures for flash memory applications.

## 2. Experimental Techniques

Ge quantum dots on Si(001) substrates were grown by solid source molecular beam epitaxy (Riber Supra 32) system using an electron gun for the deposition of thin Si buffer layer ($\sim$5 nm) with a growth rate of 0.4 Å/s and a Knudsen cell for Ge deposition, followed by the growth of a 3.0 nm Si cap layer [12]. Growth temperature was varied from 500 to 600 $^{\circ}$C and Ge monolayer (ML) thickness was assorted from 6 to 20 ML. The growth was monitored in-situ by reflection high energy electron diffraction (RHEED). On the other hand, Ge nanocrystals embedded in high-k $HfO_2$ and $Al_2O_3$ matrix on Si(100) substrates were deposited by radio frequency (13.56 MHz) magnetron co-sputtering method in $Ar+O_2$ ambient at an rf power of

50 W, similar to those reported earlier [2,13]. The as-grown sample is defined as 'A-as' and 'F-as' for Ge embedded $Al_2O_3$ and $HfO_2$, respectively. In order to grow Ge nanocrystals in high-k matrix, the sputter deposited film was thermally annealed in $N_2$ gas ambient for 30 min at 800 ºC and 900 ºC.

Ge nanowires were grown on p-Si (100) substrates by Au catalyst-assisted PLD technique in a spherical chamber. Gold catalyst was deposited on silicon substrates by thermal evaporation with thickness varying from 3 to 10 nm. Subsequently, Au coated Si was annealed at 600 ºC in $N_2$ ambient, for the formation of Au nanoparticles (nps). Pure Ge target was used as a source of Ge species using KrF excimer laser ($O=248$ nm) for the ablation on the Au-nanoparticle catalyzed Si, keeping the substrate vertically in front of the target. The laser energy density and the repetition rate were set to 2.3 J/cm$^2$ and 10 Hz, respectively. The deposition was carried out at a pressure of $10^{-2}$ mBar and the substrate temperature for growth was maintained at 600 °C. Prior to Ge deposition, Au nanoparticle coated Si (100) substrate was pre-heated at the growth temperature for 5 min. Er was incorporated into the nanowires by immersing into ethanolic solution of $ErCl_3$, $6H_2O$ of different concentrations varying from 0.01 M to 0.04 M and annealing the samples thereafter from 600 – 800 ºC in a 20% $O_2$+80% $N_2$ atmosphere for 1 hr. CdS/Ge nanowire radial heterostructure was grown on Ge nanowires templates using chemical method [14].

## 3. Results and Discussion

### 3.1 Growth and Optical properties of Ge nano-islands on Si(001)

Figs. 1 (a) and (b) show the atomic force microscopy (AFM) images of the MBE grown Ge islands  deposited for 2 (sample 'GS-1') and 5 minutes (sample 'GS-2'), respectively at a substrate temperature of 500 °C. From AFM topographic images, the variation of island shape, size and density is clearly visible. A bimodal size distribution of islands is visible from Fig. 1 (a). The average diameter (L), height (h) for larger and smaller islands are L ~ 54 nm, h ~ 18 nm and L ~ 23 nm, h ~ 7 nm, respectively for sample 'GS-1'. On the other hand, the growth of multifaceted dome like structure is evident in Fig. 1 (b) for the 'GS-2' sample with the average islands size  L ~ 90 nm and h ~ 35 nm. In Stranski-Krastanov (S-K) growth of above islands, the arrangement of deposited Ge atoms begins with the formation of a strained planar layer called the wetting layer (WL), until a critical thickness is reached. A further increase of the deposited material leads to the nucleation of three-dimensional Ge islands on the wetting-layer. At the
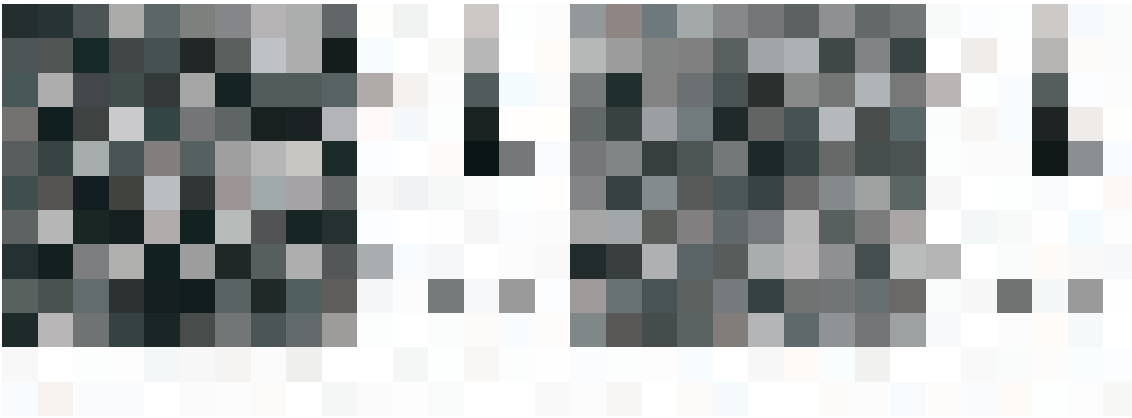
**Fig. 1.** Typical AFM topographic images for (a) 2 min. (sample 'GS-1') and (b) 5 min. (sample GS-2') grown Ge islands deposited at a substrate temperature 500 ºC.

first stage of the growth, the islands are square-based pyramids. Upon collecting more adatoms by the process of coarsening (Ostwald ripening) from neighboring islands, these pyramids transform to strained multifaceted domes. From Fig. 1 (b) it is seen that for longer time Ge deposition, the smaller islands coalesce to form multifaceted domes. One can also change the islands size and sh...

The strength ... wave functions can be enhanced i ... ains orders of magnitude below th ... spectra of self-

**Fig. 2.** 10 K photoluminescence spectra of Ge islands grown on Si substrate for sample (a) GS-1and(b) GS-2.

assembled Ge quantum dots grown at 500 °C for (a) 2 min (sample 'GS-1') and (b) 5 min (sample 'GS-2'). Broad PL peaks are observed around 0.755 eV and 0.804 eV for samples grown for 5 min and 2 min, respectively. The observed broad PL signal from Ge/Si islands is associated with the radiative carrier recombination at sharp Ge/Si interface that exhibits type-II band alignment, with a small barrier for electrons and deep potential wells for the holes confined within the Ge islands. Due to lower height (7 to 18 nm) of the islands, the PL peak of 2 min sample is blue shifted compared to sample grown for 5 min. Another cause for the shift may be due to the intermixing of Si and Ge for longer time (5 min) deposition of Ge, which reduces the band offset between islands and Si interface.

The photo-response of Ge quantum dot infra-red photodetector (QDIP) has been studied at varying temperatures. Fig. 3 shows the temperature dependent dark current–voltage (J–V) characteristics of the QDIP device [15]. The dark current density at 10 K is lower as compared to conventional infrared photo-detectors. The dark current density increases at elevated temperatures due to thermionic emissions. The fluctuations in J-V characteristic in both bias directions at 10 K are clearly observed, which reduce with increasing temperature and dies out at 40 K. This phenomenon is attributed to the carrier localisation at the Si/Si$_{1-x}$Ge$_x$ hetero-



**Fig. 3.** The dark current density-voltage characteristics of a Ge QDIP structure measured at low temperatures.

interface. These localised carriers results in an in-built-voltage ($V_b$) varying from 0.2 - 0.32V from 10 K to 300 K. One origin of this carrier localization may be due to the confined holes and large valance band offset in Ge/Si heterostructure in type II band alignment, which results in well for electrons at the Ge/Si interface in Si.

Low temperature photocurrent (PC) response was measured using a closed cycle cryostat with KBr window. The mid IR (180–220 meV) photocurrent response of the grown Ge quantum dots in the temperature range 100–300 K is shown in Fig. 4 at zero applied bias. The mid IR peak at 195 meV is redshifted with increasing temperature up to 175 K. Although the maximum photocurrent response is observed at 175 Ka shoulder peak at (205 meV) is evolved with increasing temperature, which exhibits a redshift up to 175 K. At room temperature these two peaks merge to yield a broader response. The curves in the inset of Fig. 4 show the mid IR PC response at room temperature under different -Ve bias voltages. The peak intensity increases with applied -Ve bias and saturates at -0.6 V. The photocurrent saturates when no further holes can be pumped out from the confined energy states with increasing bias. The redshift arising in PC on increasing the temperature up to 175 K is not due to Stark effect, since no peak shift is observed by applying external electrical field in both bias polarities at low and room temperatures.



**Fig. 4.** The mid-IR photocurrent spectra of capped Ge/Si QDs at different temperatures. The inset curve shows the photocurrent at room temperature under different reverse bias conditions.

The observed redshift and peak PC response can be explained by the excitonic electric field localized at the interface developed at low temperatures.

## 3.2 Electrical properties of Ge nanocrystals embedded in high-k matrices

Figs. 5 (a) and (b) show the plane-view TEM images of Ge NCs embedded in $Al_2O_3$ and annealed at 800 °C and 900 °C, respectively. The samples are hereafter referred as A-800 and A-900, respectively. The dark patches seen are Ge nanocrystals embedded in amorphous $Al_2O_3$ matrix. The nanocrystals are almost spherical and are well dispersed in the host matrix. The estimated size distribution of the nanocrystals for A-800 sample can be approximated by a Gaussian distribution with an average diameter of 7.6 nm. For A-900 sample, the distribution of the nanocrystals throughout the film is not uniform and the diameter varies from 9-17 nm. Figs. 5 (c) and (d) show the plane-view TEM images of Ge NCs embedded in $HfO_2$ and annealed at 800 °C (sample H-800) and 900 °C (sample H-900), respectively. The image resolution in Fig. 5 (d) for H-900 sample is comparatively higher. The average diameter of the Ge NCs for H-800 sample is about 3.9 nm, whereas for H-900 sample it varies from 7-13 nm. The change in Gibbs free energy of formation of GeO (111.8 kcal/mol) is much smaller than that of high-k oxides, such as $HfO_2$ (260.1 kcal/mol) and $Al_2O_3$ (378.2 kcal/mol) [16], which results in the oxidation of Hf or Al and agglomeration of Ge atoms into nanocrystals in $HfO_2$ or $Al_2O_3$ matrix during thermal annealing at high temperatures. It is observed that when annealed at 800 °C, which is well below the melting temperature of Ge (938.3 °C), only Ge nucleation occurs. Whereas for both 900 °C annealed samples (A-900 and H-900), Ge nanocrystals usually show nonuniform distribution of size and density within high-k oxide matrix due to the high diffusion rate of Ge atoms, in consistent with the previously reported results [17]. Furthermore, a higher annealing temperature is expected to result in increased critical nucleus size.

Figs. 6 (a) and (b) represent the high frequency (100 kHz) capacitance–voltage (C–V) hysteresis behavior of the MOS structures fabricated using Ge nanocrystals embedded in $Al_2O_3$ and $HfO_2$ matrix, respectively for a voltage sweep of ± 7.5 V. A negligibly small flat-band voltage shift of 0.15 V and 0.18 V is observed for $Al_2O_3$ and $HfO_2$ MOS devices without Ge NCs. However, a large memory window of 1.20 V, 6.32 V, 1.85 V and 2.38 V is observed for the A-800, A-900, F-800 and F-900 samples, respectively. This suggests that the origin of C-V hysteresis can be accredited to injected charges mainly in nanocrystals or at the interfaces between the NCs and the surrounding oxides. From the maximum flat band voltage shift of the
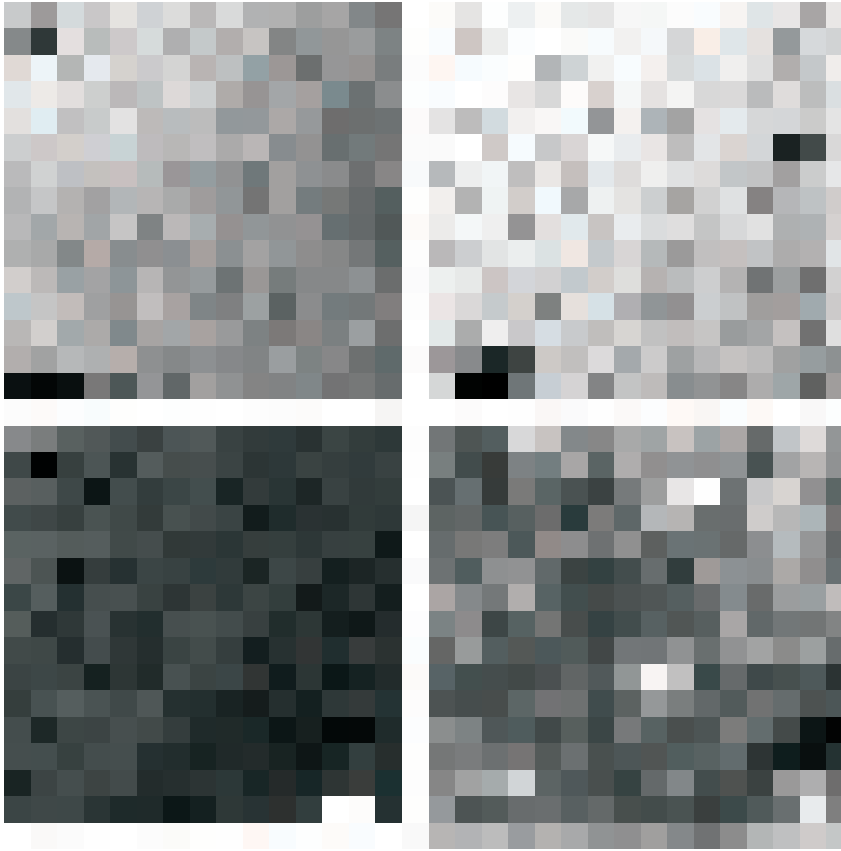
**Fig. 5.** Plan-view TEM micrograph of Ge NCs embedded in high-k matrix for (a) A-800, (b) A-

C-V curves, we have calculated the stored charge density using the following equation [18]

$$N_{charge} = \frac{\Delta V_{FB}}{\frac{q}{\varepsilon_0}\left(\frac{t_{CO}}{\varepsilon_{CO}} + \frac{t_{NC}}{\varepsilon_{NC}}\right)}$$

Where $\Delta V_{FB}$ is the flatband voltage shift, $q$ is the magnitude of the electronic charge; $t_{CO}$ and $\varepsilon_{CO}$ are the thickness and relative permittivity of the control oxide; $t_{NC}$ and $\varepsilon_{NC}$ are the diameter and relative permittivity of the nanocrystal; and $\varepsilon_0$ is the permittivity of the free space. The calculated stored charge density for the A-800, A-900, F-800 and F-900 devices are $1.4 \times 10^{12}$, $7.1 \times 10^{12}$, $4.5 \times 10^{12}$, and $5.4 \times 10^{12}$ cm$^{-2}$, respectively. The memory window and
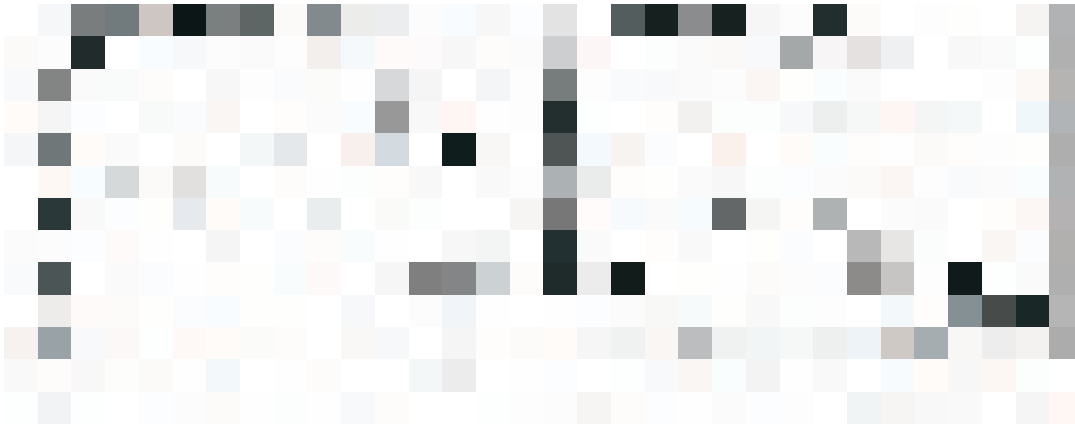
**Fig. 6.** High-frequency (100 kHz) C–V characteristics of MOS capacitor with Ge nanocrystals embedded in high-k (a) $Al_2O_3$ and (b) $HfO_2$ matrix 900, (c) F-800 and (d) F-900 samples.

stored charge density is found to be significantly enhanced on increasing the annealing temperature (900 °C) for Ge nanocrystals embedded in $Al_2O_3$ matrix as compared to that of $HfO_2$, making it attractive for nanocrystal flash memory applications.

## 3.3 Growth and optical properties of Ge Nanowires

Three different sizes of nanowires (NW) with average diameter of 30 nm, 80 nm and 130 nm have been grown by varying the size of Au nanoparticles coated on the Si wafer. The approximate Er content of Ge NWs doped using $ErCl_3$ solutions of different molar concentrations has been estimated from the energy dispersive analysis of X-ray (EDAX) in the SEM study. For the molar concentration 0.01 M, 0.025 M and 0.04 M of $ErCl_3$, the atomic concentration of Er in Ge nanowires has been found to be ∼ 0.23 %, ∼ 0.7 % and ∼ 1.15 %, respectively.

The photoluminescence of Ge NWs at room temperature in the UV-visible range has been studied using a 325 nm He-Cd laser as the exciting source. A broad PL peak in the visible wavelength around 400 nm is observed from the doped nanowires. Fig. 7(a) typically shows the UV-visible spectrum with the peak position and shape remaining the same for all the sizes investigated here. Since the size of the nanowire is not enough for significant quantum confinement, the PL peak does not originate from the quantum confinement of carriers. Since 325 nm is indirect excitation, the Er emission is attributed to the energy transfer from the Ge related oxygen deficiency centers (GeODCs), which are formed in the Ge core coating layer.

**Fig. 7.** (a) UV-visible photoluminescence spectrum at room temperature for 80 nm dia Ge nanowire % Er (b) Energy transfer scheme from GeODCs to an $Er^{3+}$ ion: the radiative transition from $T_1$ state is shown by (1); the downward arrow marked as (3) shows the 1.53 $\mu$m emission of $Er^{3+}$; the wavy arrow from $^2H_{9/2}$ to $^4I_{13/2}$ indicates nonradiative transition, while energy transfer is denoted by (2) (c) Infrared PL characteristics with different annealing temperatures. with 0.7 at. Excitation wavelength is 325 nm.

The oxygen deficiencies possess three energy states: singlet state $S_1$, triplet state $T_1$, and ground state $S_0$ [19, 20]. Due to the excitation by 325 nm (3.8 eV), GeODCs may be excited by direct absorption, which is followed by the nonradiative relaxation by phonon emission to the lower levels of triplet $T_1$ state. From here the excited carriers may relax to the ground state $S_0$ by a radiative decay : $\sim$ 400 nm (3.1 eV) light will be then emitted. Since the $T_1$ state consists of many levels, the emission is spectrally broad. This kind of emission is due to a HOMO (highest occupied molecular orbital) – LUMO (lowest occupied molecular orbital) transition, where both the HOMO and LUMO are located on the Ge atoms. A competitive process is a

non-radiative decay of the excited GeODCs to the ground state via an energy transfer to an $Er^{3+}$ion. In this way, $Er^{3+}$ ions will be excited from the ground $^4I_{15/2}$ state to the excited $^2H_{9/2}$ level, which is almost resonant with the $\mathbf{T_1}$ state. Then, the $Er^{3+}$ ions de-excites to the $^4I_{13/2}$ state by a non radiative relaxation from where a radiative transition to the ground state yields 1.53 ℿm emission. This mechanism is shown schematically in Fig.7(b). Fig. 7(c) shows the room temperature infra-red PL spectra of Er-incorporated Ge nanowires as a function of annealing temperature. It may be noted that indirectly excited emission is quenched for annealing temperatures lower than 600 °C. The $Er^{3+}$induced luminescence intensity increases with the annealing temperature from 600 °C to 750 °C. The intensity is found to decrease with a further increase of annealing temperature to 800 °C. This observation indicates that under non-resonant excitation, the Er ions are excited by the energy transfer from GeODCs as we have discussed. Basically, a minimum annealing temperature of 600 °C is necessary to form a local non-centrosymmetric coordination environment around the $Er^{3+}$ ions. These GeODCs are abundant till an annealing temperature of 750 °C resulting in the strong enhancement of the $Er^{3+}$ related PL at 1.53 ℿm. With further increase in the annealing temperature in an $O_2$ ambient, stoichiometric $GeO_2$ is gradually formed from $GeO_x$ leading to the depletion of GeODC defects. Therefore, the decrease of the number of GeODCs causes the reduction of $Er^{3+}$ PL above 750 °C. At these high temperatures, the indirect excitation mechanism is almost disappeared and thus Er can be excited only by direct resonant absorption processes as it was shown in stoichiometric $GeO_2$. It is interesting to note that the width of the Er emission peak depends on the excitation mechanism: pumping resonantly (980 nm) leads to a reduced line width of the central 1.53 ℿm emission peak compared to non-resonant pumping. A possible explanation can be related from a site selection in the indirect Er excitation.

We also performed measurements by using the 980 nm excitation wavelength which is resonant with an internal transition ($^4I_{11/2}$ to $^4I_{15/2}$ state) of the $Er^{3+}$ ions. With this excitation condition no energy transfer from GeODCs to Er ions occurs. Fig. 8(a) shows the 1.53 ℿm Er PL intensity variation with Er doping concentration for typical Ge NWs of 30 nm average diameter and annealed at 750 °C. It is observed that the PL intensity enhances with increasing the doping percentage. It is possible that the increased doping of Ge nanowires lowers the symmetry of the $Er^{3+}$ ion/host structure leading to an increase of the number of optically active $Er^{3+}$ ions. Despite the high doping, Er clustering is not present. The inset of Fig. 8(a) shows the variation of the 1.53 ℿm PL intensity with the laser flux for resonant excitation (980 nm). No saturation of the Er related emission occurs. This contrast with other observations: Er
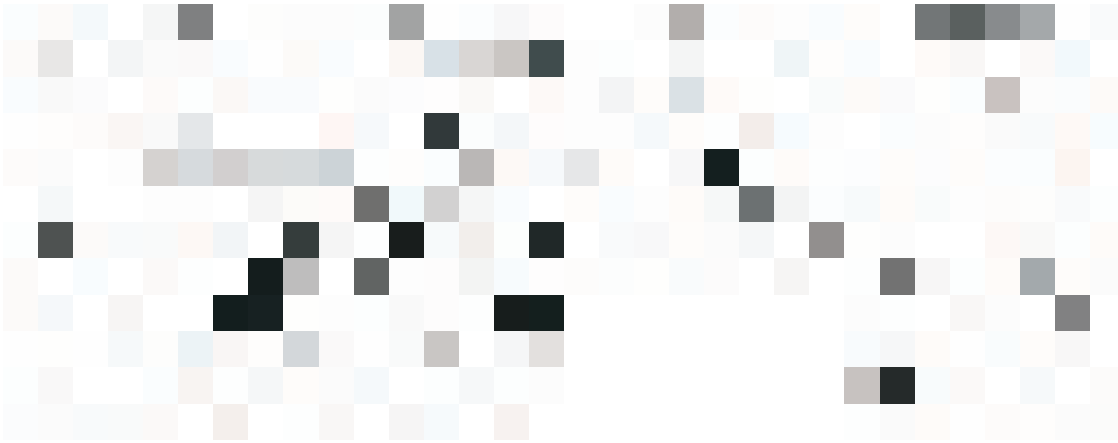
**Fig. 8. (a)** Er-induced PL emission of 30 nm dia Ge nanowires with different Er concentration. Inset shows the Er-induced 1.53 $\mu$m PL peak intensity as a function of photon flux.

**Fig. 8. (b).** PL decay of 1.53 $\mu$m Er emission peak for laser excitation power of 11.12 and 303.0 mW for 30 nm dia 0.23 at % Er doped Ge nanowire.

doped Si system shows a sub linear power dependence of the emission due to the saturation of the optically active $Er^{3+}$ ions [21] or to localized Auger quenching. Here it emerges that the excitation phenomena of $Er^{3+}$ ions in Ge NW are different than in Si.

We have studied the time-resolved photoluminescence characteristics of the Er emission peak excited by the 980 nm diode laser. The experimental decay curves and fits for 30 nm wide Ge NWs doped with 0.23 at. % Er for two different powers is shown in Fig. 8(b). The decay curves could be best fitted using a stretched exponential [22]

$$I_{12}(t) = I_c \exp\left(\left(\frac{t}{t}\right)^B\right)$$

where $\Omega$ and $E$ are the life time parameter and dispersion parameter, respectively.

The mean life time $< \Omega >$ can be calculated from the following relationship :

$$! \ \Omega \quad \frac{\Omega}{E} * \left(\frac{1}{E}\right)$$

where $*$ denotes the Gamma function.

The derived lifetimes are 5.0$\pm$0.3 ms and 3.6$\pm$0.1 ms, respectively, for an excitation

power of 11 mW and 303 mW. It may be noticed that these lifetimes are as long as for Er doped Si nanocrystals within silica matrix. The change of lifetime at 1.53 $\mu$m for Er-doped Ge NWs with the pump power is related to the variation of the Er emission cross section. A decrease of the radiative lifetime induces an increase of the emission/absorption cross sections. This leads to the variation of the Er PL signal. The decrease in lifetime at higher power can be explained by an up-conversion effect due to the interaction between two neighboring Er$^{3+}$ ions both excited to the first excited state. In the interaction process, one de-excites to the ground state and the other is promoted to the $^4F_{7/2}$ level or $^4F_{5/2}$. Depending on whether this doubly excited ion will decay back to the first excited state or to the ground state, the up-conversion interaction depletes the first excited state population. This up-conversion interaction depends strongly on the excited Er concentration. Another mechanisms which might have an effect on the lifetime, is the non-radiative recombination paths such as defects in the oxide matrix (here the Ge related oxygen vacancies) and the excited state absorption, when an excited Er$^{3+}$ ion absorbs a pump photon promoting to the higher excited state. The defect related non-radiative recombination might be the major reason of the lifetime change with power in our case.

## 3.4 Growth and optical properties of Ge/CdS nanowire heterostructures

Figs. 9(a) and 9(b) show plane-view bright field TEM micrographs of Ge nanowires and a single Ge/CdS nanowire heterojunction, respectively [14]. The diameter of VLS grown Ge nanowires at 850 $^o$C (Fig. 9a) is estimated to be 80-100 nm. The bottom inset in Fig. 9(a) shows the magnified TEM image of a typical Ge nanowire, revealing the formation of a core-shell structure of core diameter 60 nm and shell thickness 10 nm. The shell consists of a thin GeO$_2$ layer, which is commonly observed in Ge nanowires and may be formed due to the surface oxidation of nanowires during ex situ characterization. The selected area electron diffraction pattern (SAD) recorded in the core region clearly indicates the growth of single crystalline Ge, as shown in the upper inset of figure 9(a). Figure 9(b) represents the typical TEM micrograph of a single Ge/CdS radial heterojunction nanowire of total diameter 250 nm, indicating the attachment of CdS nanoparticles on Ge nanowires. The surface of CdS shell appears quite rough due to high growth rate in chemical bath deposition. The SAD pattern (upper inset of the figure) of the Ge/CdS nanowire surface shows distinct circular rings, indicating the formation of polycrystalline CdS. The dominant diffraction rings are indexed as (111), (220) and (311) planes of cubic CdS. The high-resolution TEM image (HRTEM), in lower inset of the figure, shows the lattice fringes owing to nanocrystalline grains of CdS.
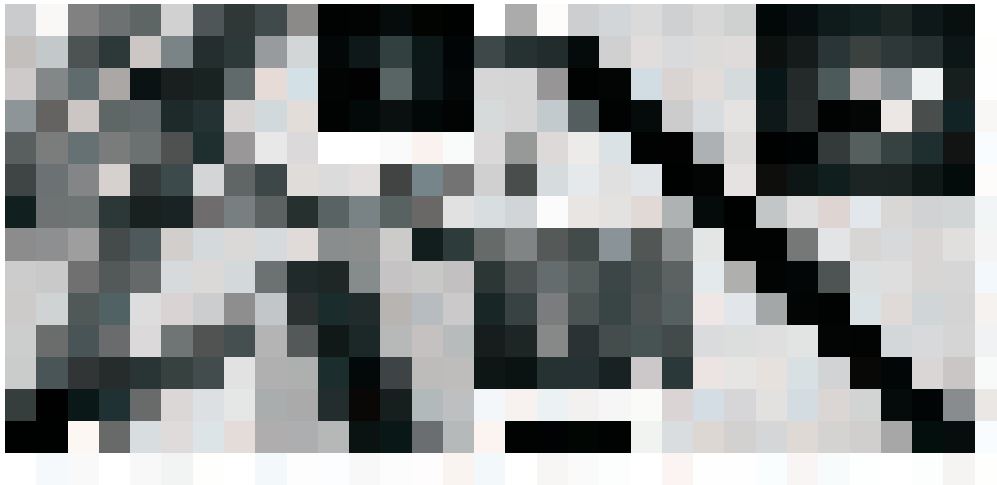
**Fig. 9.** Bright field TEM image of (a) Ge nanowires of diameter 80-100 nm. Inset (below) indicates the formation of a thin $GeO_2$ (10 nm) on the surface of nanowire having diameter $\sim$ 60 nm. Inset (top) represents SAD pattern at Ge core region. (b) a typical Ge/CdS radial heterostructure nanowire of diameter 250 nm. Inset at top right shows the SAD pattern of Ge/CdS heterostructure. HRTEM image at a portion of CdS shell region, indicating lattice images of nanocrystalline grains (inset at bottom left).

Electrical characterizations of Ge/CdS nanowire heterojunctions were performed using two different lateral electrode configurations (device-I and device-II) at room temperature. Fig. 10 shows the room temperature dark I-V characteristics of Ge/CdS radial nanowires. It may be noted that the control Al/Ge nanowires/Al device shows Ohmic behavior (not shown here). The possible formation of Ohmic contact between Al and Ge nanowire is mainly due to the presence of a thin $GeO_x$ oxide layer on the nanowire surface. The device with both contacts on CdS shell (device-I) shows a symmetric I-V nature in forward and reverse bias voltages, which is presented in Fig. 10. This is plausible since CdS makes Ohmic contact with Al. Interestingly, the I-V characteristics of device with one contact on CdS and the other on Ge nanowire (device-II) is remarkably different and a diode-like behavior is clearly observed. This asymmetric I-V nature reveals the formation of radial junction between CdS shell and Ge core though the reverse saturation current is quite high. The high leakage current in CdS-Ge nanowire heterojunction may be due to high interfacial defects and surface recombination rates of bath deposited CdS shells of the radial junction causing significant minority carrier generation at 300K. It may be noted that Ge nanowire is not intentionally doped, which may result in a rather weak junction potential. Inset of figure 10 shows the I-V characteristics of the device-II in reverse bias mode

**Fig. 10.** I-V characteristics of Ge/CdS nanowires under dark condition (device-I and -II). Inset shows the dark and photocurrent characteristics of Ge/CdS nanowires (device-II) under reverse bias. The schematic diagram of device-II is shown in upper inset.

under dark and illumination from a broad band light (100 mW/cm$^2$) source. Fascinatingly, under illumination, the reverse current increases dramatically due to the photo-induced generation of minority carriers in device-II. The increase of current for device-I is quite less as the origin is due to photoconductive component only. For example, the dark and photocurrent for device-II are -4.0 $\times 10^{-6}$ and -2.6$\times 10^{-4}$ A ( at -2V), respectively, as compared to -8.2$\times 10^{-5}$ and -1.2$\times 10^{-4}$A (at -2V) for device-I. Photosensing characteristics of Ge/CdS core-shell nanowires to white light for the device configurations I & II are shown in Fig. 11. It is observed that the response time of device-II is remarkably faster than device-I with enhanced current modulation. The study demonstrates that the core-shell Ge/CdS nanowire heterojunction may be attractive for photodetection, optical sensing and switching devices.

Fig. 12 presents the photocurrent spectrum (under zero bias) of Ge/CdS nanowire junction (device-II) in comparison to control CdS thin film. The photocurrent of Ge/CdS core-shell nanowire junction is almost two order higher, having broader spectral response than that of nanocrystalline CdS film synthesized by the same method. Therefore, electron-hole pairs generated in the nanowire heterojunctions are collected efficiently under the built-in junction field. The presence of a thin GeO$_2$ on the surface of Ge nanowires (shown in TEM micrographs) may be useful to contribute higher photocurrent due to formation of a p-i-n like junction. The

**Fig. 11.** Photoresponse characteristics of Ge/CdS core-shell nanowires for device-I and -II under illumination of white light.

**Fig. 12.** Photocurrent spectrum of Ge/CdS nanowire heterojunction in comparison to bath deposited control CdS film.

photoresponse of Ge/CdS core-shell junction is quite strong up to 800 nm as compared to 650 nm for CdS film and is extended till 1000 nm, the long wavelength limit of the broad band source. The strong photoresponse in the wavelength range 700-900 nm, which is above the energy gap of bulk Ge, may be attributed to a combination of quantum confinement in Ge nanowires and the presence of sub-band gap interfacial defects in CdS-Ge heterojunction. The enhanced spectral bandwidth and photocurrent in broad wavelength range (450-1000 nm) signifies that Ge/CdS core-shell nanowire heterojunction can be attractive for photovoltaic devices.

### 3.5 Nickel nanocrystals for floating gate MOS memory devices

Nickel has gained much popularity in CMOS technology for application as a silicide contact, trapping layer, and metal gate electrodes, since it creates a deep quantum well for the trapping of charge carriers for its high work function [23]. Owing to high work function ($\sim$ 4.9 eV), Ni nanocrystals result in deep quantum well for the trapping of charge carriers.

The memory structures used in this study were MOS capacitors with a dielectric stack consisting of Ni nanocrystals sandwiched between a tunneling $SiO_2$ and high-$k$ and capping high-$k$ layers. Memory capacitors with a trilayer capacitors of $Al_2O_3$/Ni/$SiO_2$/Si (ANSS), and $HfO_2$/Ni/$HfO_2$/Si (HNHS) were fabricated.

Detailed information about the nanostructures growth after annealing of the middle Ni
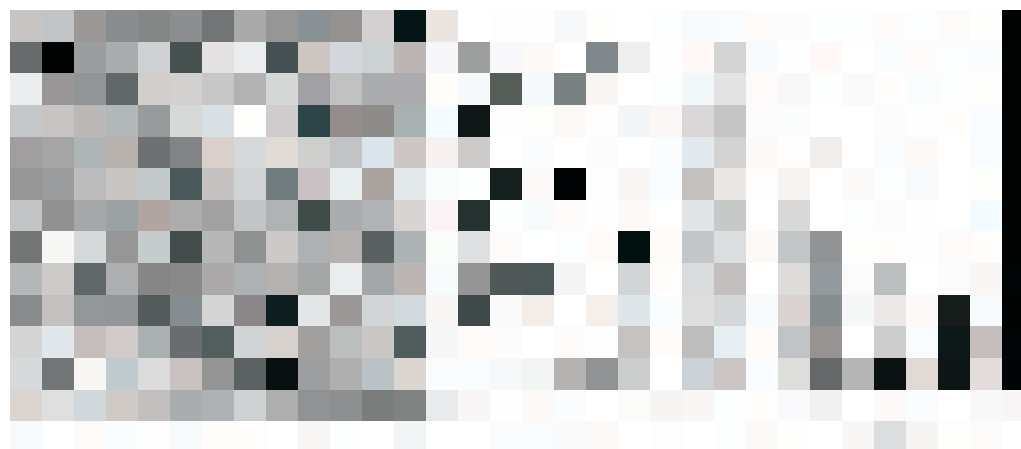
**Fig. 13.** (a) Plan view HRTEM image and (b) size distribution of the 950 °C, 5 minute annealed nickel nanocrystals in SiO$_2$ matrix.

layer was obtained by plan view HRTEM studies. Fig. 13.(a) shows the surface morphology of the Ni film on SiO$_2$ after annealing at 950 °C for 5 minutes. It's clearly shows the formation of isolated nickel nanocrystals of different size distributions. The size distribution of metal nanocrystals is estimated from the HRTEM micrographs and is shown in Fig. 13(b). The average diameter of the nanocrystals varies from 6 nm to about 22 nm with Gaussian size distribution. The maximum numbers of particles ($3.5 \times 10^{13}$ dots cm²) of 12 nm were observed from the TEM micrograph. When the annealing time of the film is increased to 15 minute at same temperature 950 °C, the average size of nanocrystals decreases slightly as shown in Fig. 14. In this case the average particle size distribution ranges from 4 nm to about 22 nm with the maximum size distributions of about $3.85 \times 10^{13}$ dots/ cm² at 10 nm, as shown in Fig. 14(b). A much improvement in the uniformity of size distribution is observed on increasing the annealing temperature to 1000 °C. We observed a very good uniformity of the isolated nanocrystals with smaller size and distributions after annealing the films at 1000 °C for 5 minutes, as shown in the plan view HRTEM micrograph in Fig. 15. Fig. 15(a) shows the low resolution view, whereas Fig. 15(b) shows the high resolution view of the films. The high magnification HRTEM image of a single Ni nanocrystal is shown in the inset of Fig. 15(b). The lattice fringes appears to consist of single crystal domains and exhibits d-spacing of 0.12 nm corresponding to the {220} lattice spacing of nickel. The average diameter of the nanocrystals ranges from 3 nm to 6 nm, having a large distribution of nanocrystals of about $1.3 \times 10^{14}$ dots/ cm² at 4 nm shown in Fig. 15(c). The gaps between the particles are of the order of 2-5 nm. The coalescence of
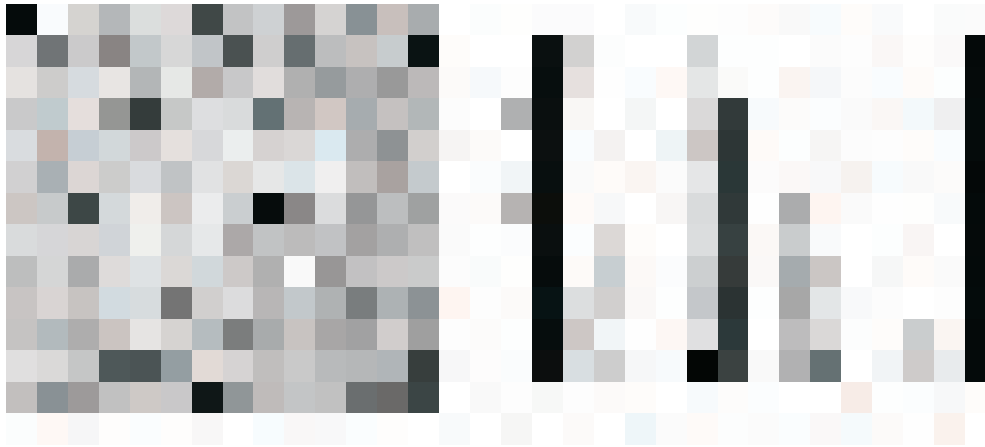
**Fig. 14.** (a) Plan view HRTEM image and (b) size distribution of the 950 °C, 15 minute annealed nickel nanocrystals in $SiO_2$ matrix.
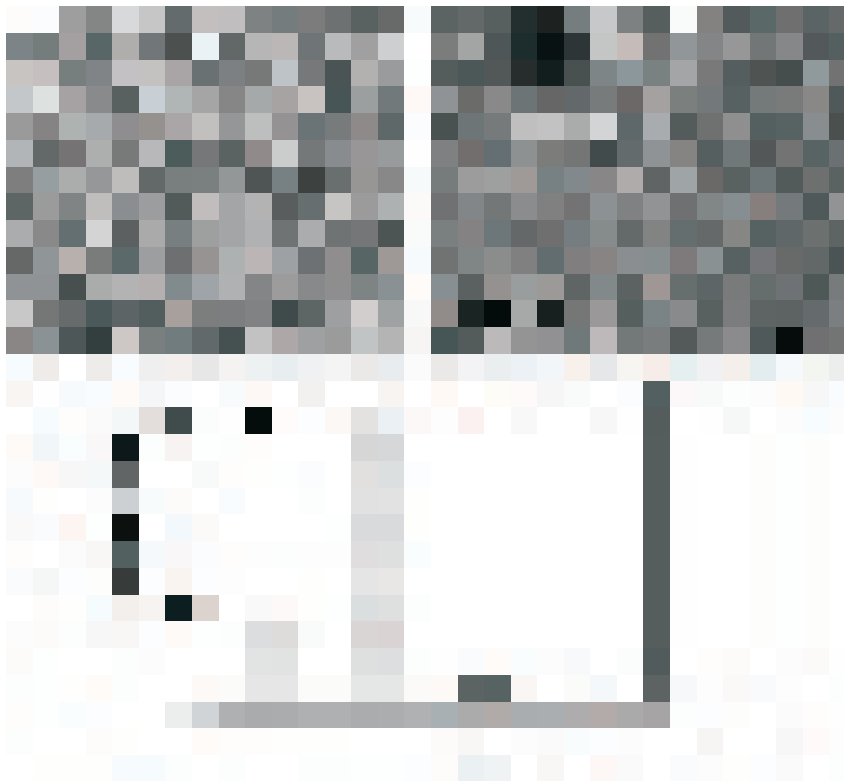


**Fig. 15.** Plan view HRTEM image of the 1000 °C, 5 minute annealed nickel nanocrystals (a) Low resolution view (b) high resolution view; inset shows the single nickel nanocrystals and (c) size distributions.

nanocrystals is observed with further increase the annealing time for 1000 °C, 15 minute. Typical cross-sectional HRTEM micrograph of the 1000 °C 5 minute, annealed HNHS memory structure is shown in Fig. 16. The micrograph clearly shows the formation of isolated and spherical Ni-NCs, which are confined within the intermediate layer located away from the $HfO_2$/Si interface, shown in inset of Fig.16. The average diameter of the NCs is found to be $\sim 8$ nm. The creation of Ni NCs may be attributed to the formation of Ni nanoclusters on $HfO_2$ layer during evaporation of ultrathin Ni film. The average density of the NCs is found to be $9.3 \times 10^9$ cm$^{-2}$ for the as-deposited samples. The Ni NC density reported here is much lower as compared to the previous reports of Ni NC on $HfO_2$ and Ru NC on $Al_2O_3$/$SiO_2$. This indicates that nucleation behavior of metal nanocrystals on $HfO_2$ is slow, which may be due to the low nucleation rate in a thermal evaporation as compared to chemical vapour deposition process [24]. However, the memory devices with such low nanocrystals densities have been reported earlier [25]. The subsequent post-deposition annealing (PDA) in $N_2$, results in the increase of crystallite sizes and improvement of crystalline quality of the nanocrystals.
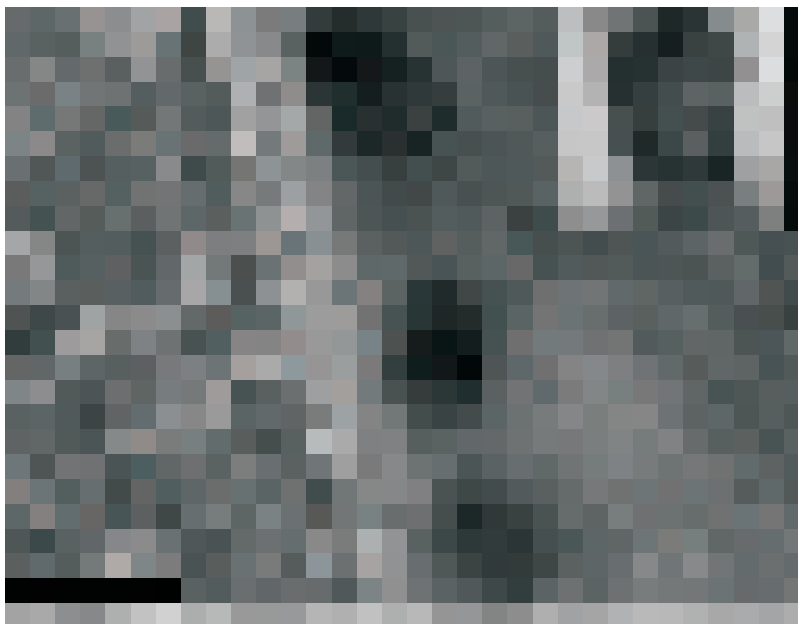


**Fig. 16.** HRTEM image of the 1000 °C, 5 minute annealed $HfO_2$/Ni/$HfO_2$/Si MOS capacitors (Inset shows single Ni-NC).

Fig. 17 (a) shows the high frequency C-V hysteresis characteristics of trilayer MOS capacitors having ANSS structures with and without Ni-NCs at different annealing conditions, measured at room temperature by sweeping the gate voltage ($\pm 9$ V) from accumulation to inversion region and then sweeping back. As can be seen from the figure, a very small hysteresis width is observed for the control and as-deposited samples compared to the nanocrystals embedded samples. The maximum memory window have been observed for the 1000 °C, 5 minute annealed samples for the charge trapping in the tiny isolated nickel nanocrystals. CV characteristics at different sweeping voltage of the 1000 °C, 5 minute annealed samples are shown in Fig. 17(b). It is clearly observed that the hysteresis width increases from 1.66 V to 3.7 V with the increase of sweeping voltage from $\pm 5$ V to $\pm 15$ V respectively. The results demonstrate that the Ni nanocrystals are attractive as the trapping nodes for floating gate memory devices.



**Fig. 17.** (a) C-V characteristics of different annealed MOS devices having ANSS structure; (b) C-V of 5 minute annealed MOS devices as a function of sweeping gate voltage.

## Summary and Conclusions

In the present review, a compendium of systematic investigation on group-IV semiconductor nanostructures carried out in our group for the development of silicon compatible charge storage, Coulomb blockade, mid-IR photodetector, light emitters and other photonic devices has been discussed. We have presented the structural and optical characteristics of Ge islands grown on Si (100) by molecular beam epitaxy. The observed infra-red photoluminescence signal at 10 K from Ge islands is associated with the radiative recombination of holes confined in the Ge islands and electrons localized in the Si buffer layer. The temperature and bias

dependent photocurrent spectra of a capped Si/SiGe/Si (001) QDIP photodetector device are presented. We have also grown Ge and Ni nanocrystals (4 – 18 nm in diameter) embedded in $SiO_2$ and high-k $Al_2O_3$ and $HfO_2$ matrices for applications in floating gate memory devices. The observed shift in flatband voltage for C-V curves of MOS structures  has been attributed to electron trapping in embedded Ge nanocrystals.

One dimensional Er-doped Ge nanowires and core-shell Ge/CdS radial nanowire heterostructures have been fabricated by VLS technique.  Defect induced photoluminescence emission due to GeODCs leads to a carrier mediated pathway for Er excitation for non-resonant excitation (325 nm) for $Er^{3+}$ ions. For resonant excitation with 980 nm, an increase of optically active $Er^{3+}$ ions for a given nanowire diameter has been achieved. The average lifetime of 1.53 $\mu$m Er emission has been found to vary from 3.6 ms to 5 ms. An enhanced photoresponse with broad spectral bandwidth was observed in core-shell nanowire devices in the wavelength range 450-1000 nm. The observed photoresponse can be essentially useful for fabricating broad band photovoltaic and photodetection devices based on nanowire heterojunctions. The compatibility of  silicon-based nanostructures with planar integrated circuit technology makes them attractive for next generation nanoelectronic and nanophotonic devices with ultrafast switching speed, high storage density and unique  optical properties.

## Acknowledgement

## References

1.  C. J. Park, K. H. Cho, W. –C. Yang, H. Y. Cho, S.-H. Choi, R. G. Elliman, J. H. Han and C. Kim, Appl. Phys. Lett. 88, 071916 (2006).

2.  S. Das S, K. Das, R. K. Singha, A. Dhar, and S. K. Ray  Appl. Phys. Lett. 91,  233118 (2007).

3.  K. Das, M. NandaGoswami, R. Mahapatra, G. S. Kar, A. Dhar, H. N. Acharya, S. Maikap,  J-H. Lee , and S. K. Ray,  Appl. Phys. Lett. 84, 1386 (2004).

4.  L. C Kimerling, Appl. Surf. Sci. 159, 8 (2000).

5.  J. S. John, J. L. Coffer,.; Y. D. Chen, R. F. Pinizzotto, J. Am.Chem. Soc. 121, 1888 (1999).

6.  B.O.Dabbousi, M.G. Bawendi, O.Onitsuka, M.F. Rubner, Appl. Phys. Lett 66, 1316 (1995).

7.  N. Tessler, V. Mededev, M. Kazes, S. H. Kan, U. Banin, Science 295, 1506 (2002).

8.  C. Bechings, S. Ferrer, A. Zaban, J. Sprangue, B. A. Gregg, Nature 383, 608 (1996).

9.  V. Pardo-Yissar, E. Katz, J. Wasserman, I. Willner, J. Am. Chem. Soc. 125 (2003).

10.  H.L. Hanafi, S. Tiwari and I. Khan, IEEE Trans. Electron Devices, 43,  1553, (1996).

11.  J. D. Blauwe, IEEE Trans. Nanotechnology, 1, 72, (2002).

12.  R. K. Singha, S. Das, S. Majumder, K. Das, A. Dhar and S. K. Ray, J. Appl. Phys. 103, 114301 (2008).

13.  S. Das, R. K. Singha, S. Manna, S. Gangopadhyay, A. Dhar and S. K. Ray, J. Nanopart. Res. DOI 10.1007/s11051-010-0054-8,(2010).

14.  S. P. Mondal and S. K. Ray, Applied Physics Letters, 94, 223119  (2009).

15.  R. K. Singha, S. Manna, S. Das, A. Dhar, and S. K. Ray, Applied Physics Letters, 96, 233113 (2010).

16.  CRC Handbook of Chemistry and Physics, 70th ed. Aready-Reference Book of Chemical and Physical Data, R. C. Weast, D. R. Lide, M. J.  Astle, and W. H. Beyer, Eds., CRC, Boca Raton, Florida (1990).

17.  X. L. Wu, T. Gao, X. M. Bao, F. Yan, S. S. Jiang, and D. Feng, J. Appl. Phys. 82, 2704 (1997).

18.  S. Tiwari, F. Rana, H. Hanafi, A. Hartstein, E. F. Crabbe and K. Chan, Appl. Phys. Lett. 68, 1377 (1996).

19.  A. Kanjilal, S. Tsushima, C. Götz, L. Rebohle, M. Voelskow, W. Skorupa, M. Helm, J.Appl. Phys., 106,  63112 (2009).

20.  L. P. Ginzburg, A. A. Gordeev, A. P. Gorchakov, A. P. Jilinsky,  J.Non-Cryst. Solids 183, 234 (1995).

21.  A. Polman, D.C. Jacobson, D.J. Eaglesham, R.C. Kistler, J. M. Poate,  J. Appl. Phys. 70, 3778   (1991).

22.   L. Pavesi, M. Ceschini, Phys. Rev. B 48, 17625 (1993).

23.   D. Panda, A. Dhar and S.K. Ray, IEEE Trans. Electron Devices,  55, 2403 (2008).

24.   Z. Tan, S. K. Samanta, W. J. Yoo, and S. Lee,  *Appl. Phys. Lett.*, 86,  0131071 (2005).

25.   J. Dufourcq, P. Mur, M.J. Gordon, S. Minoret, R. Coppard, T. Baron,  *Materials Science and Engineering C*, 27, 1496 (2007).

# 98th Indian Science Congress

**January 3-7, 2011, Chennai**

# II

ABSTRACT OF

# PLATINUM JUBILEE LECTURE

# PLATINUM JUBILEE LECTURE

## Utility and Novelty of Nanofluids for Thermal Engineering Applications

**Indranil Manna[a,b]**

[a]Central Glass and Ceramic Research Institute,
Jadavpur, Kolkata–700 032
[b]Department of Metallurgical and Materials Engineering,
IIT Kharagpur, W.B. 721 302,
*Email : imanna@cgcri.res.in*

Nanofluids are engineered stable colloidal suspension of nanometer sized ($<100$ nm) metallic/ceramic solids (particles, rods, fibers) in conventional heat transfer fluids in a small quantity ($<1$ vol %). The usually high thermal conductivity of nanofluid has led to continued experimental and theoretical studies to evaluate its utility. Despite the sustained effort, the genesis and mechanism of this enhanced thermal transport property of nanofluid is not yet established. Some researchers believe that the results showing anomalous enhancement in thermal conductivity is a result of random over-estimation, lack of consistency methods of nanofluid preparation, and systematic error in measurement techniques. While mechanisms such as existence of nano-layer at liquid/solid interface, phononic heat transfer, Brownian motion and clustering of nanoparticle have been modeled to justify the enhancement but none of them has been universally accepted to be the ultimate cause for enhancement in thermal conductivity.

In this lecture, a comprehensive overview of the systematic approach to prepare nanofluids following single- and two-step methods using metallic/ceramic nanoparticles and their constitutional characterization and thermal property assessment will be presented. The experimental data will be validated by suitable comparison with that predicted by the existing theoretical models. The thermal conductivity of nanofluids is observed to be strongly dependent on parameters like concentration and size of nanoparticles, temperature of measurement and stability of dispersion. Metallic nanofluids show better enhancement as compared to ceramic dispersed nanofluids at much lower concentration, smaller size and also exhibit better stability. Ceramic nanoparticle dispersed nanofluids are cheaper and show considerable enhancement at low concentration. Brownian motion and clustering of nanoparticles seem to have strong influence

on thermal conductivity enhancement. The viscosity of ceramic nanofluids exhibit very interesting behavior and shows lower values (than base fluid) at low concentrations and higher values at higher concentrations. This kind of an observation has been rarely reported in literature and the mechanism behind this will be discussed.

# 98th Indian Science Congress

**January 3-7, 2011, Chennai**

# III

ABSTRACT OF

# YOUNG SCIENTIST AWARD PROGRAMME

# YOUNG SCIENTIST AWARD PROGRAMME

## Synthesis and Enhanced Photoluminescence in Novel $Au_{Core}$Au-$Ag_{shen}$ Nanoparticles Embedded $Nd^{3+}$-doped Antimony Oxide Glass Hybrid Dichroic Nanocomposites

**Tirtha Sam**

Glass Science and Technology Section, Glass Division,
Central Glass and Ceramic Research Institute, CGCRI
196 Raja S. C. Mullick Road, Kolkata–700 032, India

$Au_{core}$Au-$Ag_{shen}$ nanoparticles and $Nd^{3+}$ ion co-doped in a novel antimony(III) oxide based dielectric (glass) matrix was synthesized for the first time, by a new very simple single step methodology involving selective thermochemical reduction without employing any external reducing agent. These nanocomposites are dichroic in nature. They were characterized by the evolution of UV-Vis-NIR absorption and photoluminescence spectra, XRD patterns, TEM and SAED images. XRD and SAED indicate the building of core-shell nanoparticles through the formation of (111) and (200) planes whereas TEM advocates the generation of spherical and spheroidal particles of 21-107 nm sizes. Photoluminescence upconversion exhibits two major emission bands of $Nd^{3+}$ ions at 540 (green) and 649 (deepred) nm which undergo about 5 fold intensity enhancement by the nanoparticles. Such plasmonic enhancement is attributed to the local field enhancement and energy transfer from plasmonic Au-Ag nanoparticles to $Nd^{3+}$ ions. These nanocomposites have many nanophotonics applications.

# 98th Indian Science Congress

**January 3-7, 2011, Chennai**

# IV

# ABSTRACT OF

# SYMPOSIUM/INVITED LECTURE

### 1.    Solar Photovoltaics- Status Review

#### K. L.  Chopra

Former Director, Indian Instuitute of Technolgy, Kharagpur
Founder, Thin Film Laboratory,
IIT Delhi & Microscience Laboratory, IIT Kharagpur

Solar photovoltaics is a multi -billion dollar global sun- rise industry which   has been growing   by  well over 30%  every year  for the  last several years ( before the  global meltdown).Global production of  solar cells  per year has already crossed 3500 MW equivalent. Photovoltaics  now find widespread applications  from small stand alone  power supplies to  60 MW power stations.  The technology   continues to be primarily (over 90%)  dominated  by standardized and reliable monocrystalline and multicrystalline  silicon based . Despite large scale  production, the price of crystalline Si cells has not decreased below $3/ W , largely because  of the high  cost of Si wafers . Major  industrial efforts  are being made to  manufature thin-film microcrystalline , nanocrystalline  and hybridized Si - based solar cells.Amorphous Si  thin-film technology which at one time  was considered the most promising  contributes only about 4% (about 100 MW) to the   global production today. The price of relatively much lower efficiency a-Si thin-film cells  is also comparable to that of crystalline Si cells. Nevertheless,

such cells    find applications in    special areas  as building integrated  photovoltaics. After considerable research and development efforts , thin-film CdTe  based solar cell technology has finally reached a large scale production  of  over 100 MW at  production cost of over \$1 / W by a single manufacturer. The thin-film  CIGS based  solar cell technology , though more complex, has also  advanced considerably and  may   be able to compete with  CdTe technology on \$/W basis. Presently , intensive  research is being carried out to develop   novel organic / polymeric materials, organic-inorganic composites  ,and dye-sensitised  materials  for solar cells  with an indication of  a promising future of economically viable and cheaper technologies. The viability of  any one or more of such technologies will ultimately  be determined by the criteria of manufacturabilty, cell  efficiency, stability and life of the cells and , above all , by the cost  per watt. The Review will discuss the present status of the various PV technologies and  their future prospects.

## 2.      Semiconductor Sources of Terahertz Radiation: Principles, History and Trends

**M. S. Kagan[1], I. V. Altukhov[1], V. P. Sinis[1], I. N. Yassievich[2],
S. K. Ray[3] and J. Kolodzey[4]**

[1]Institute of Radioengineering and Electronics of RAS,Moscow
[2]A.F. Ioffe Physico-Technical Institute of RAS,St.Petersburg
[3]Department of Physics & Meteorology IIT Kharagpur, India
[4]University of Delaware, Newark, DE, USA

The terahertz frequency range (1-10 THz) of electromagnetic radiation is of special interest in many applications. THz radiation can be used for remote ecological monitoring, global meteorological observations, radar systems, space-based astronomy, medicine, molecular spectroscopy, and many other fields. Nevertheless, the THz range has long remained undeveloped, mainly due to the lack of compact, tunable and efficient coherent sources. In this report, the short review of development of ideas, experimental realizations and up-to-date tendencies, including the results of intensive research performed during the last two decades, will be given.

The presently available solid-state sources of coherent THz radiation include quantum cascade lasers, which can operate now at frequencies down to 1.9 THz without magnetic field and 1.39 THz with magnetic field, and *p*-Ge hot-hole lasers, which operate at high electric and magnetic fields due to inversion in the energy distribution of free holes. These semiconductor lasers, developed in the mid-1980s, operate at 100- to 300-?m wavelengths and helium

temperatures in the pulsed mode. The THz lasing has been obtained also for intra-impurity optical transitions in optically pumped n-Si and in strained p-Ge and single-QW SiGe/Si structures under strong electric field pumping.

Note, that all semiconductor THz lasers operate at cryogenic temperatures and cannot work at room temperature ($kT=25$ meV) because the energies of quanta in THz range are around 10 meV and to obtain the population inversion is practically impossible. So, we need to reject the laser scheme and to look for another way to get THz generation at room T. The reasonable idea seems to look for a semiconductor system with a fast negative differential conductivity (NDC), which can produce THz oscillations in a suitable resonant cavity. Such systems will be considered, as well.

**3.    A New Type of Fuel  Cell for  Conversion of High Temperature Heat to  Electricity without Carnot  Limitation**

**K. T. Jacob**

Department of Materials Engineering,
Indian Institute of Science,
Bangalore–560 012

A new type of solid oxide fuel cell (SOFC) will be presented which is capable of converting heat absorbed from a high-temperature source to electricity bypassing the Carnot limitation. The essential cell reaction is the partial oxidation of carbon to carbon monoxide, unlike in the case of conventional SOFC where oxidation of hydrogen and carbon monoxide to water vapour and carbon dioxide are the main reactions. The fuel cell is endothermic and will absorb heat from an external source and convert it to electricity. The theoretical basis of the new fuel cell will be explained and some preliminary experimental results will be presented. A liquid metal is used as the medium for the carbon-oxygen reaction generating carbon monoxide. There is no violation of the second law of thermodynamics since the theoretically loss free conversion of heat to electricity is accompanied by a chemical reaction.

**4.    Excitements and challenges in advanced materials research by non-equilibrium processing**

**B. S. Murty**

Department of Metallurgical and Materials Engineering
Indian Institute of Technology Madras,
Chennai–600 036, India
*E-mail : murty@iitm.ac.in*

Advanced materials such as nanocrystalline materials, bulk metallic glasses and high entropy alloys have attracted the attention of both academicians and industrialists in recent decades. There are a number of routes for the synthesis of these materials. One of these is high energy ball milling or high kinetic energy processing. This is a non-equilibrium processing route, which can lead to materials that are significantly far from their equilibrium configurations, and thus can have significantly different properties in comparison to conventional materials. In fact, it is possible that in case of nanocrystalline materials, those synthesized by this route can have different properties from those prepared from other routes, though their grain size is the same, due to the differences in the nature and density of defects present. Similarly, amorphous materials and high entropy alloys synthesized by this route could have different structure and hence properties from those developed from other routes. This not only gives opportunities to develop materials with exciting properties by this route but also can take us deeper into the understanding of the behavior of materials far from equilibrium. However, the processing of the materials by this route poses engineering challenges and opportunities that need to be addressed for it to be more widely accepted. The present talk will deal with the excitements and challenges in this field based on the research being carried out at the laboratory of the speaker.

**5.    Complexities of metal nanoparticle – hydrogen interaction: basic issues and novel applications**

**B. R. Mehta**

Department of Physics,
Indian Institute of Technology Delhi
New Delhi–110 016, India

Interaction of hydrogen with Rare Earth (RE) and Palladium (Pd) is probably one of the most widely studied solid surface- gas molecule interaction due to complex physical and chemical

processes involved and its direct relevance in important hydrogen technologies. In case of nanoparticles, size and surface dependent modifications in the electronic and structural properties make this interaction even more complex. The novelty of our research approach has been to separate the interfering effects of hydrogen induced topographical, structural and electronic changes by a precise control of nanoparticle size and interparticle separation. A novel integrated approach, based on in-flight size selection, compaction and crystallization, has been used for the synthesis of size selected, monosized, monocrystalline and spherical nanoparticles In case of RE metals, a continuous and reversible 'structural, optical and electronic' transition between reflecting metallic dihydride and transparent semiconducting trihydride states on hydrogenation makes hydrides of RE metals suitable for switchable mirror applications. In our laboratory, we have conceptualized the usage of nanoparticle characteristics for solving some of the nagging material problems inhibiting the performance of switchable mirror devices. 'nanoparticle route' has been used for achieving an 'all-round' improvement in the switching characteristics of a 'new generation' of Gd and Pr nanoparticle based switchable mirrors in comparison to previously reported thin film, RE-Mg alloys and mutilayers.. Interaction of hydrogen with Pd thin films, nanocrystalline layers, size-selected nanoparticle and nanorod structures have been studied. By controlling the nanoparticle size and separation, geometrical effects due to lattice expansion during hydride formation and electronic effects due to H incorporation have been controlled and separated. Based on the improved understanding of the gas- solid interaction, this study resulted in a 'proof of concept' for developing a new type of hydrogen and deuterium sensor having a pulsed response with fast response of the electronic effect and high sensitivity of the topographical effect. These results have wide ranging importance in the research areas related to hydrogen switching, storage, sensing and condensed matter nuclear science.

## 6.    Oxide nanoparticles for application is alternative energy storage systems

**Amreesh Chandra**

Department of Physics and Meteorology,
Indian Institute of Technology,
Kharagpur-721 302
*Email : achandra@phy.iitkgp.ernet.in*

Carbon dioxide emission and global warming are amongst the major challenges facing the mankind in the $21^{st}$ century. Any future energy landscape will have to be less dependent on

fossil fuels and increase use of renewable and cleaner energy sources. Amongst renewable sources: solar, wind, tidal and bioenergy have attracted massive attention. But, for a country like India, solar and bioenergy seems to be most viable. Even when the use of renewable sources is widely anticipated, their applications are limited because of two reasons, namely: high cost and the intrinsic intermittent nature. Therefore, alternative energy storage systems will have to be an integral and important constituent of the future energy landscape. Amongst the storage systems, supercapacitors and lithium ion batteries are most promising. This talk will focus on one such storage device i.e., 'supercapacitors'.

The most important components of a supercapacitor are the electrodes, ion conducting membrane and the electrolyte. Amongst the electrode materials being used in commercially available supercapacitors, $RuO_2$ and graphite/ carbon black are most common. But both of these suffer from serious drawbacks; while $RuO_2$ is toxic and expensive, graphite puts a limit to the maximum specific capacitance which can be achieved. Therefore it has become essential to search for alternative electrode materials.

$MnO_2$ has recently received much attention in energy storage systems and is seen as a possible cheap alternative to $RuO_2$. It is known that an increase in surface area of electrode material results in an increased capacitance of the resultant system, however the extent of this increase may be dependent on a number of factors. This talk will present couple of methods to prepare the nanoparticles of $MnO_2$. After careful and detailed characterization using techniques like BET, XRD, SEM, TEM, etc. the synthesized $MnO_2$ powders have been used as electrode material in supercapacitors. $MnO_2$ is embedded in a polymer matrix to achieve flexibility in design and engineering of storage devices. Performance of fabricated supercaps will also be presented in this talk.

## 7.    Nanostructured Coatings

**A. K. Tyagi**

Surface and Nanoscience Division,
Materials Science Group
Indira Gandhi Centre for Atomic Research,
Kalpakkam–603 102, Tamil Nadu, India

Nanocrystalline semiconducting oxides (ZnO, $SnO_2$, $In_2O_3$), ceramic oxides

($TiO_2, Al_2O_3, ZrO_2$) and nitrides (GaN, CrN, TiN, TiAlN) are technologically important materials. A vibrant program on synthesis of nanocrystalline powders and nanostructured coatings is being pursued at IGCAR. A large number of nanomaterials like $Al_2O_3$, $CeO_2$, $ThO_2$, CaO, $Cr_2O_3$, $TiO_2$, $ZrO_2$, CrN, TiN, AlN, TiAlN and $SnO_2$ have been synthesized by different methods. Oxides have been prepared by temperature programmed decomposition of metal nitrates, carbonates, oxalates and hydroxides as well as by soft chemistry routes in aqueous and non-aqueous mediums. Using an in-house developed TGA-EGA-MS system, each decomposition stage of precursors were monitored by subjecting them to linear heating under different atmospheres. For synthesis of nitrides like CrN and TiN, we used direct gas phase nitridation of corresponding nano oxides in reactive atmosphere ($NH_3$). Various nanostructures of GaN like wires and belts are produced by vapour-liquid-solid CVD tecgnique. $TiO_2$ nanorod arrays were synthesized by anodization of Ti. The techniques used for obtaining monolithic nanocrystalline thin films are combustion CVD, plasma CVD, laser pyrolysis, spray pyrolysis, pulsed laser ablation and electron beam PVD. Multilayer architectures are obtained through magnetron sputtering and constructed out of alternate nanometric layers like TiN/TiAlN. XRD, XPS, FT-IR, LRS, PL,TEM, SEM, AFM and SIMS are used for characterization. The present talk will give an overview of our activity highlighting applications of these nano powders, thin films and nanostructured coatings.

## 8. Synthesis of nano materials by thermal plasma technology

### S. K. Singh

Institute of Minerals and Materials Technology
Bhubaneswar–751 013, INDIA
*E-mail : sarojksingh@gmail.com*

In recent years, there has been considerable interest in the preparation of nano particles due to their enhanced chemical, mechanical, electrical, optical and magnetic properties opening up a new range of potential uses and applications for these advanced materials. Many processes are being developed currently for preparation of nano materials. Amongst the various methods used for synthesis of nano powders, the plasma processing appears to be most promising. Thermal Plasma with high temperature gas-phase chemistry within the plasma environment provides an attractive route for nano powder synthesis. Plasma synthesis has several important advantages relative to various other powder synthesis techniques. The peak temperature is

higher than that of any other method; the energy density is high; and cooling in the flow direction is rapid. It is possible to retain high temperature metastable phases. Relatively high throughput can be achieved in a small reactor. The controlled atmosphere of a plasma reactor is conducive to producing powders of exceptional purity, especially in case of radio frequency (RF) reactors, as these operate without electrodes. Post synthesis milling, a major contamination source for conventionally produced powders, is not required because the process inherently produces sub-micron particles. There is virtually complete chemical flexibility in contrast to many other advanced methods. For example, flame synthesis necessarily involves oxygen, laser synthesis requires reactants which have strong radiative transition corresponding to high power (usually $CO_2$) lasers, spray pyrolysis and sol-gel techniques are limited to reactants which can be formulated as appropriate solutions. This paper describes a brief review of various thermal plasma methods employed for preparation of nano particles such as SiC, AlN, CNT etc.

### 9.    Near net shape development of components by direct laser cladding

**Jyotsna Dutta Majumdar**

Indian Institute of Technology,
Kharagpur-721 302

Direct laser cladding is a technique for the development of component by melting materials in the form of powders and wires using a high power laser and subsequently depositing it on a dummy substrate in a layer by layer fashion to build the desired shape of the component. A rapid processing speed, retention of metastability in the microstructures, environment friendliness and the scope of automation are the notable advantages associated with direct laser cladding. In the present contribution, direct laser cladding has been applied for development of alloys, metal matrix composite and compositionally graded coupons. The materials of investigations were AISI 316L stainless steel, SiC dispersed AISI 304 stainless steel composite, in-situ TiB dispersed ?-Ti matrix composite and cobalt layers on Ti-6Al-4V with a graded interfaces. Direct laser cladding was conducted by melting metals/alloys powders by high power continuous wave Diode laser with a beam diameter of 3.4 $\times$ 2.4 mm and its deposition on the base substrate to develop coupons of dimensions 20 mm $\times$ 20 mm $\times$ 10 mm. Laser processing was carried out using Ar as shrouding environment to protect the surface against oxidation. In all the cases, it was observed that optimization of laser parameters is essential to ensure a defect

free microstructures with homogeneous composition and phase distribution. Grain size, and phase distribution of the developed coupons were found to vary with The effect of process parameters on microstructures and properties were investigated. The mechanical and electro-chemical properties of the direct laser clad coupons were found to be superior to that of conventionally available one.

## 10. Electrical, optical and magnetic properties of oxide based systems and their nanostructures

**M. S. Ramachandra Rao**

Department of Physics,
Nano Functional Materials Technology Centre and Materials Science Research Centre
Indian Institute of Technology (IIT) Madras,
Chennai-600 036
*E-mail : msrrao@iitm.ac.in;*

Oxide electronic material systems offer ample opportunities to probe in to their electrical, optical and magnetic behavior upon doping. The functionality of nanoscale oxide electronic devices is controlled by novel engineered nanomaterials. In this talk, I will give a short review of our recent results on magnetic nanoparticles and multiferroic systems. The main focus of the talk will be on ZnO based systems. ZnO is a unique material that offers a number of application possibilities as the ZnO lattice is amenable to metal ion doping (3d and 4f) and the physics of doping in ZnO is very interesting [1]. Doping a small amount of transition metal ion changes the morphology as well as optical properties of the parent ZnO compound. For example, Ni doping in ZnO results in a dramatic decrease in electrical resistivity of bulk ZnO and a similar trend is seen in the case of a few other 3d metal ion doped ZnO compounds. The talk will also present results on the bulk, thin film and nanostructured growth of ZnO, by diverse growth techniques, that could be used in devices [2]. I will present our latest results on the realizing of stable p-type conductivity in codoped ZnO in codoped ZnO and the magnetic behavior therein. I will also briefly touch upon our results on magnetic nanoparticles and magnetoelectric coupling in doped bismuth ferrite [3].

1. Shubra Singh, N. Rama and M.S.Ramachandra Rao. Appl. Phys. Lett. Appl. Phys. Lett. 88, 222111 (2006).

2. Shubra Singh et al. J.Phys. D.Appl.Phys. (Topical review) 40 (2007) 6312.

3. B. Ramachandran, A. Dixit, R. NAik, G. Lawes and M.S.Ramachandra Rao, Phys.Rev.B 82 (2010) 012102.

## 11. Ion Beam Synthesis of buried Au and Ag Nanoparticle layers in $SiO_x$

**S. K. Srivastava[1], S. A. Khan[2], Pravin Kumar[2] and D. K. Avasthi[2]**

[1]Department of Physics and Meteorology,
IIT  Kharagpur-721 302
[2]Inter-University Accelerator Centre,
New Delhi-110 067

Insulator-buried two-dimensional layers of metallic nanoparticles are very promising for guiding light in ultra-fast, all-optical devices. Ion beam demixing between metal atoms and the insulator in oxide/metal/oxide layers deposited on a substrate has been proved to be a very effective tool to synthesize such structures. However, the attempts using $\sim$ 100 keV ions required post-irradiation annealing on one hand [1, 2], and those using $\sim$ a few MeV ions resulted in nanoparticles surrounded by smaller halo clusters on the other. For the latter, the long range recoils arising due to large nuclear energy loss ($S_n$) are reported to cause the halo formation, while for the former we infer that the $S_n$ is too little to produce a collision cascade sufficient for providing metal-atom diffusion to aggregate into nanoparticles. In this contribution, we report the employment of ions of 350 keV, intermediate between the two energies, to irradiate $SiO_x/Au/SiO_x$ and $SiO_x/Ag/SiO_x$ structures with oxide thicknesses of 40 nm and metal layer thicknesses of 5 and 12 nm, and subsequent synthesis of clean nanoparticles without the need of any annealing step. We have observed a systematic and considerable blue shift in the plasmon resonance peaks with increasing ion fluence, not attributable merely to the change in nanoparticle size. We propose a model describing the discontinuous nature of as-deposited metal layers and their ion-induced nanoclustering, as revealed by TEM micrographs, to explain the corresponding UV-VIS absorption spectra with respect to the Mie theory of light scattering by particles. The blue shift has been parametrized with an effective matrix dielectric constant $?_M$, which is found to decrease in an exponential manner with ion fluence.

**References :**

1. P. Gangopadhyay, R. Kesavamoorthy, K.G.M. Nair, and R. Dhandapani, J. Appl. Phys. **88**, 4975 (2000).

2.   S. Dhara, R. Kesavamoorthy, P. Magudapathy, M. Premila, B.K. Panigrahi, K.G.M. Nair, C.T. Wu, K.H. Chen, and L.C. Chen, Chem. Phys. Lett **370**, 254 (2003).

## 12.   Novel oxidation techniques for growth of ultra-thin SiO$_2$

### Nandita Dasgupta

Department of Electrical Engineering,
IIT Madras, Chennai

Thermally grown SiO$_2$ has been unprecedented in quality and reliability so far and is predominantly used as the gate dielectric for silicon MOSFETs. However, the semiconductor road map expects that the thickness of gate SiO$_2$ layers will be reduced to 0.8–1.3 nm for 8 Gb devices causing the leakage current density to exceed beyond the allowable limit of 1 A/cm$^2$ in thermally grown ultrathin SiO$_2$. Further, even though high-k dielectric material is expected to replace SiO$_2$ as the gate for next generation MOSFETs, still an extremely thin interfacial SiO$_2$ layer is required before the deposition of the high-k dielectric in order to achieve an acceptable interface quality. This has initiated a lot of research in recent years to develop alternative techniques for realizing ultrathin SiO$_2$. In this presentation two such alternative techniques, namely Chemical and Laser-induced oxidation will be highlighted.

Chemical oxidation in diluted nitric acid solutions at and below room temperature has been carried out to grow ultra thin oxides in the thickness range from 1.7 nm to 2.4 nm. When the chemical oxidation was followed by anodic oxidation, the electrical and reliability characteristics of MOS devices showed tremendous improvement. MOSFETs with gate oxide grown by this technique have demonstrated low subthreshold slope, high transconductance and channel mobility. Chemical oxidation by subjecting the samples to HNO$_3$ vapour has also been carried out to realize thinner oxides (#1 nm).

Laser induced oxidation (LIO) of silicon has also been carried out to grow ultrathin oxide using a pulsed Nd-YAG laser. The effects of oxygen partial pressure, dc discharge and duration of LIO on the characteristics of MOS devices with gate oxide grown by LIO have been studied in detail. Devices grown in O$_2$ : N$_2$ : 3 : 1, for 60 s in the presence of dc discharge are found to have the best characteristics in terms of breakdown field strength, time to breakdown and leakage current. It has been shown oxide thickness in the range of 0.86 nm can be grown with good control using this technique.

### 13.   Thin film photovoltaics : Advances beyond silicon

**Udai P. Singh**

School of Electronics Engineering
KIIT University, Campus-3, Patia
Bnhbaneswar-751 024, India

Current trends suggest solar energy will play an important role in future energy production. Silicon has been and remains the traditional solar cell material of choice. The present total market share of crystalline silicon is more than 80%. While silicon is a highly abundant material, it requires an energy intensive process to purify and crystallize. In an effort to circumvent the materials resource limitations and production costs associated with the first generation silicon technology, effort is being applied toward the development and production of PV cells based on advanced technologies. Recently commercial interest is beginning to shift towards thin film solar cells. Material, manufacturing time and weight savings are driving the increase in thin films. The thin-film technologies will continue to have to compete with crystalline silicon (c-Si) in the future as they do now.

Promising competitors of silicon in the solar energy market are found in lower- cost thin-film materials. Thin-film solar cells will become an important resource for our sustainable energy supply in the near future. At present, several thin film PV technologies are available with different properties in terms of efficiency, maturity, stability and applicability. The prominent among them are copper chalcopyrite thin films like copper indium gallium diselenide (CIGS) and cadmium telluride (CdTe). The present article will focus on $Cu(In,Ga)Se_2$ thin film solar cells. The copper-chalcopyrite alloy class of thin films exhibits bandgap-tunable p-type semiconductor behavior that can be effectively used in solar-energy conversion devices. A significant advantage of such thin-film solar cells is the small amount of material needed and the relatively low cost of the materials required. Apart from low material costs, deposition of copper chalcopyrite films can be accomplished at lower temperatures than that of crystalline silicon, ultimately decreasing the manufacturing costs. The chalcopyrite solar cells also have benefits over crystalline silicon-based counter parts due to their opto-electronic material properties, particularly a direct bandgap and high absorption coefficient. Copper chalcopyrite films lessthan1 mm in thickness can absorb a substantial fraction of the incident viable photons (with energies exceeding the optical bandgap), resulting in thin-film cells that can be extremely efficient and also light weight. If deposited on suitable substrates, they can in addition be

flexible, expanding the application range beyond the confines of conventional rigid crystalline silicon solar cells. Of additional importance, the versatility of the copper- chalcopyrite alloy film class, in particular the tunability of bandgap with different alloy compositions, allows for the development of novel and alternative solar-energy conversion configurations.

The present R&D is focused on improving efficiency, gaining a thorough understanding of the material properties and developing new deposition techniques. The present paper discusses the current status, prospects and challenges faced in the CIGS based solar cell.

## 14. Advanced Wide Bandgap Semiconductor Nanostructures for Optoelectronics

**K. Baskar**

Crystal Growth Centre,
Anna University,
Chennai–600 025, INDIA
*E-mail : baskar@annauniv.edu*

Gallium nitride (GaN) and zinc oxide (ZnO) are promising wide bandgap semiconductor materials for optoelectronics devices particularly light emitting diodes (LEDs) and laser diodes (LDs) in the ultraviolet (UV) and visible region of electromagnetic spectrum in addition to their potential to harness solar energy with high conversion efficiency. These materials can also be used in high-power, high-frequency and high-temperature electronics and spintronics applications. Preparation of semiconductor materials in the form of nanostructures is important to maximize the density of states for the fabrication of high-efficient quantum functional devices due to their low structural dimensions.

Gallium nitride (GaN), indium gallium nitride (InGaN) and aluminum gallium nitride (AlGaN) two dimensional semiconductor nanostructure were grown by metalorganic chemical vapour deposition (MOCVD). Light emitting diodes (LEDs) were fabricated and studied. The effects of growth temperature, group-V/nitride ratio, thickness of low temperature nucleation layer, doping concentrations on the structural, optical and electrical characteristics of the materials were discussed. The potential of these material structures for the fabrication UV LEDs and biosensors to detect prostrate cancer has been discussed.

ZnO nanostructures such as nanorods, nanowalls and nanochains were successfully synthesized using high-pressure pulsed laser deposition (PLD). The vertically well aligned ZnO

nanorods were obtained on Si substrate at 650 °C in the oxygen pressure of 7 Torr. Influence of substrates on the morphology of ZnO nanorods was studied by depositing ZnO on GaN (0001), $Al_2O_3$ (0001) and Si (100). The close lattice match between ZnO and GaN leads to the dense columnar growth of ZnO film followed by lateral growth of nanowalls, whereas well separated nanorods were observed on a large lattice mismatched Si substrate. In addition to the substrate effect, the doping of specific element, particularly, magnesium (Mg) influences the morphological transition of ZnO from nanorods to nanochains. The effect of Mg concentration and the substrate temperature on the growth of ZnO nanochains were discussed. The high aspect ratio, good vertical alignment, low screening effect and better crystallinity of the tapered ZnO nanorods exhibited promising field emission performance at low turn-on field of 2 V/$\mu$m with a high current density of 7.7 mA/cm$^2$, and a large field enhancement factor. A growth mechanism has been proposed to explain the morphology of low dimensional structures of ZnO.

GaN nanocrystals were synthesized using Ga-EDTA and ammonia at a temperature between 600 and 900 °C. GaN nanotips were grown on sapphire substrate at 1000 °C using simple thermal evaporation and condensation method. The cobalt was doped with GaN nanoparticles to study the dilute magnetic semiconductor (DMS) behavior of the materials. The Magnetic measurements were carried out by superconducting quantum interface device (SQUID) magnetometer. The magnetic measurement confirmed the existence of ferromagnetic behavior both at 10 and 300 K. The experimentally calculated field enhancement factor was 425 which confirms the suitability of GaN nanotips for field emitter applications.

Nanostructures have been characterized by atomic force microscopy (AFM), scanning electron microscopy (SEM), transmission electron microscopy (TEM), X- ray diffraction (XRD), photoluminescence (PL), Fourier transform infrared analysis (FTIR), Raman spectroscopy, hall measurements and positron annihilation. The results have been discussed in detail.

# 98<sup>th</sup> Indian Science Congress

**January 3-7, 2011, Chennai**

# V

ABSTRACT OF

# ORAL/POSTER PRESENTATION

1. ZnO nanoparticles decorated on functionalized (f-CNTs) and Sensoric Applications

E. Manikandan[*,1], S. Sinha Ray[1], A. Maity[1], M. Maaza[2],
U. Kamachi Mudali[3] and A. K. Tyagi[4]

[1]Nanotechnology Innovation Centre,
National Centre for Nanostructured Materials (NCNSM),
Meiring Naude Road,
Council for Scientific & Industrials Research (CSIR),
PRETORIA, South Africa
[2]Nanoscience Laboratories, Materials Research Dept,
iThemba Ion Beam Lab-NRF, South Africa
[3]MSG, Indira Gandhi Centre for Atomic Research (IGCAR),
Kalpakkam–603 102, Tamilnadu, India
[4]CSTS, RPMRR & DD, IGCAR Technology Transfer Cell,
Kalpakkam–603 102, Tamilnadu, India

The hybrid ZnO : CNTs nanocomposites was successfully fabricated by attaching ZnO nanoparticles with various diameter. The as prepared agglomerate ZnO nanoparticles were dispersed uniformly in the range of few nanometer (nm). The ZnO : CNTs nanocomposites were synthesized by simple wet chemical (sol-gel) derived from zinc acetate [$CH_3(COO)_2$. $2H_2O$] onto functionalized multi-wall carbon nanotubes (f-MWCNTs) at low temperature 80

°C. The quantity of ZnO exposure on the CNTs can be turned and reliant upon the ZnO precursor concentration. A possible growth mechanism based on the surface diffusion of as-deposited precursor on the CNTs has been proposed. The X-ray diffraction (XRD) pattern, Raman Spectroscopy (RS), field emission-scanning electron microscope (FE-SEM) and high resolution transmission electron microscope (HRTEM) techniques indicate the uniform nanocrystalline vista of the ZnO particles. The SEM and TEM results of ZnO particles has homogeneously deposited along the complete periphery of CNTs. The ZnO : CNTs nanocomposite hybrid materials were further characterized by RS, photoluminescence and UV-Visible spectroscopy studies at room temperature (RT). The results from XRD, PL and RS confirm the characteristics wurtzite structure, emission peak and E2 phonon mode assigned pure and functionalized hybrids. The ZnO/CNTs composite PL spectrum shows blue-shift and vibrational RS spectra significance shown red-shift is due to the nanoscale particle size of the deposited ZnO compared to the bulk. The amount of ZnO coverage on the MWCNTs can be tuned and is dependent upon the ZnO precursor concentration.

## 2.    Nanosize effects on structural and electrical properties of Zn modified PZT

**[1]S. K. S. Parashar, [2]Kajal Parashar  and  [3]B. S. Murty**

[1, 2]School of Applied Sciences;
KIIT University,
Bhubaneswar-751 024
[3]Department of Metallurgy and Materials Engineering
Indian Institute of Technology, Madras,
Chennai–600 036, India
*[1]E-mail : sksparashar@yahoo.com*

The synthesis and control of materials in nanoscale leads to improve physical properties as well as device performances. Nanocrystalline ferroelectric materials have attracted considerable scientific interest in view of their unusual physical properties arising out of particle size effect. The impact of the dielectric constant on system performance has triggered research for search of materials with high dielectric constant. Nanocrystalline Lead Zirconate Titanate $Pb(Zr_{0.53}Ti_{0.47})O_3$ (PZT), with high dielectric constant 34000 has been synthesized by high energy ball mill technique (mechanical alloying). Materials exhibit novel behavior when their size falls below the critical length 50nm scale. We observed consequence, phenomena such as phase transition, surface and interface effects and changes in the lattice symmetry effects

(Tetragonal to Cubic) on by reduction in size (10nm). It is evident from Impedance Spectroscopy that the relaxation time of unsintered sample Zn Modified PZT (PZZT) is less than that of sintered one. It is also observed that PZZT samples have less relaxation time than the others rare earth modified (Gd, Nd, Sm) PZT. It has been observed that modified PZT have less relaxation time than the unmodified PZT. As crystallite size increases on increasing sintering temperature, the dynamics of the process slows down. ZnO play as grain refinement in PZT which hinders the grain growth.

### 3. Fabrication of Metal and Metal Oxide Sponges by Self-Bubbled Triton X – 165 hydrogel templates

**Farid Khan**

Nanomaterials Discovery Laboratory,
Department of Chemistry
Dr. H. S. Gour University,
Sagar–470 003, India
*E-Mail : faridkhan58@yahoo.com, farid.fk@rediffmail.com*

A novel method was used to fabricate Ag, Au or CuO monoliths via thermal treatment using Triton X – 165 as a sacrificial template. Continuous network of pores with sizes varied from 50 nm – 10 $\mu$m can be prepared through the use of additives such as dextran, silica nanoparticles and the swelling agents, 1,3, 5 trimethylbenzene (TMB), suggesting that the use of Triton X – 165 gel offers a versatile route to the preparation of intact inorganic structures with controlled morphology. Scanning electron microscopy (SEM), Thermogravimetric analysis (TGA), Powder X – ray diffraction (PXRD) and Brunauer – Emmitt and Teller (BET) surface area studies were used to characterize these materials. The specific surface area of Au/Triton X – 165/dextran determined 8. 26 m$^2$g$^{-1}$.

**4.    Breakdown/Microwave Characteristics of 12 GH$_Z$ n-Si/p-Ge and n-Ge/p-Si Heteoro Junctions**

**S. P. Pati[1], P. R. Tripathy[2], M. Mukherjee[3] and S. K. Choudhury[2]**

[1]Emeritus Professor, National Institute of Science & Technology,
Berhampur, Odisha
[2]School of Physics, Sambalpur University,
[3]Inraphel, Calcutta University
*E-mail : prof_sppati@yahoo.co.in*

A p-n junction under reverse bias avalanche breakedown condition is capable of producing high frequency rf power in Impatt mode. With the advancedment of Device Technology, the present state of art reports realization of alloy Si-Ge allow junction, Si-Ge hetero junction for different electronics systems. The computer aided study of avalanche breakdown and microwave characteristics of the two complementary hetero junctios of the form n-Si/p-Ge and n-Ge/p-Si, has been reported in the scope of this paper which also provide a comparative account of these hetero junctions with corresponding Si and Ge homo junctions. Interesting results could be observed. The Breakdown Voltage and Electric Field become maximum for Si Homo Junction. However the device efficiency is sufficiently pushed in case of both the hetero junctions. All the diodes show optimum frequency around 12 GH$_Z$. The peak negative conductance and diode negative conductance and diode negative resistance register the highest values for n-Ge/P-Si hetero junction amongst the four junctions indicating possible realization of high rf power delivery at high efficiency for this structure.

**5.    Simulation of electrical characteristics of organic molecules for nanoelectronic devices**

**P. Aruna Priya, C. Preferencial Kala, C. Muthamizhchelvan
and D. John Thiruvadigal***

Department of Electronics and Communication Engineering
Center for Materials Science and Nanodevices
SRM University, Kattankulathur–603 203, India
Department of   Physics and Nanotechnology;
Center for Materials Science and Nanodevices
S.RM University, Kattankulathur–603 203, India
*\*E-mail : djthiruvadigal@ktr.srmuniv.ac.in*

Theoretical understanding of electron transport phenomena through single molecules is

of great importance for the design of future devices and materials in molecular electronics. In this paper, we report the electronic transport property of molecular wires by a molecular orbital theory on the basis of Extended Huckel Theory (EHT) and the non-equilibrium Green's function (NEGF) formalism. The wires consist of three kinds of molecules, pyridine, pyrazine, pyrimidine and pyridazine which are attached to the atomic scale semi-infinite gold $<111>$ electrodes. Our calculation reveal that the relative position of the double nitrogen atoms in the molecular rings can significantly affect the transport behavior due to change in the electronic structure of the molecule and the current characteristics of pyrazine exhibits an ohmic character on a large range. The effect of quantum interference and coupling are investigated in detail.

## 6. Analysis of Multi wall carbon nano tubes based Nanocomposite using Taguchi Analysis in Grinding Process

**S. Prabhu[1] and B. K. Vinayagam[2]**

[1]Assistant professor (Sr.G), School of Mechanical Engineering,
SRM University, Chennai-603 203
[2]Professor & Head, Department of Mechatronics Engineering,
SRM University, Chennai-603 203
*E-mail : prabhume@yahoo.co.in, bkvei23@yahoo.com*

Recent developments in nanocomposites have opened up new avenues for different arena by many means. Carbon nanotubes is one of the most exciting nanostructural materials and their excellent mechanical properties of high strength to low weight ratio, high young's modulus of 1 Tpa and low density of 2.0 g/cm$^3$ makes them as a viable reinforcing phase in a variety of polymer, ceramic, and metallic matrices to design high-performance nano composite materials. CNTs could be an ideal reinforcing phase to design aluminum matrix composites to improve Al alloys wear and creep resistance. In this paper prepared the nano composite of LM 25 Aluminum alloy and carbon nano tube by stir sand casting process and conducted tribological tests like friction and wear analysis. L9 orthogonal array was used to optimize the machining parameters in Taguchi method. Analysis of variance (ANOVA) and F-test were used to determine the significant parameter affecting the output parameters. XRD analysis is used to predict the stress intensity level of nanocomposites. SEM analysis is used to find the nanocomposite surface morphology. Results showing that the nanocomposite increase the high strength to low weight ratio, hardness is decreased with carbon nano tube based nanocomposites.

**7.    Influence of poly(ether imide) on the thermo-oxidation of poly(ether ether ketone)**

**R. Ramani and S. Alam\***

Polymer Science Division, D.M.S.R.D.E.,
G.T. Road, Kanpur–208 013, India

We report here the two-step thermo-oxidative degradation kinetics in a miscible high performance polymer blend poly(ether ether ketone)/poly(ether imide) (PEEK/PEI) with various compositions. Interestingly, the PEI addition is found to enhance the thermo-oxidation rate of PEEK. The effective activation energy (Ea) as a function of conversion (a) is found using model-free kinetics (MFK) which reveals that the blend with 50% PEI content show high Ea value and the DSC results corroboratively show a significant change in crystallinity for this PEI composition. Based on these results, the blend with composition 50/50 (PEEK/PEI) is suggested to have optimum thermal stability.

**8.    Synthesis of supported layered double hydroxide adsorbents for defluoridation of water**

**Sujata Mandal, Shilpi Saxena, Rahul Kumar and S. Mayadevi**

Chemical Engineering and Process Development Division,
National Chemical Laboratory,
Dr. Homi Bhabha Road,
Pune–411 008

Layered double hydroxides (LDHs) were supported on agricultural waste materials viz. coconut coir and areca nut fibers and the adsorption properties of these supported materials for fluoride adsorption were studied. Two different supported LDHs (Zn/Al and Mg/Al) were prepared and the effect of preparation method (co-precipitation in aqueous medium, direct deposition), relative metal concentrations and nature of support on the fluoride adsorption capacity was studied. Supported LDH prepared by direct deposition method exhibited higher fluoride adsorption capacity compared to unsupported LDH and that prepared by co-precipitation method.

9. **The Surface Modified ZnO Thick Film Resistor by CuO as room Temperature H$_2$S Gas Sensor**

**M. K. Deore[1], V. B. Gaikwad[2] and G. H. Jain[3]**

[1]Dept. of Physics, Arts, Commerce and Science College,
Ozar (Mig)–422 206, (M.S).
[2]K.T.H.M. College, Nashik–422 005, (M.S.),
[3]Arts, Commerce and Science College,
Nandgaon–423 106, (M.S.),
*[1]E-mail : deoremadhav@rediffmail.com*

The thick films of pure ZnO were prepared by screen printing technique, CuO modified thick films were obtained by dipping them in to 0.01 M aqueous solution of CuCl$_2$ for 20 min time interval. In which cu$^{2+}$ could be incorporated as an additive in to ZnO base material. The films were fired at 550 °C for 30 min. The surface morphology and element analysis of the films were studied by SEM and EDAX. The gas response of pure and surface modified film were studied for different gases CO, Cl$_2$, NH$_3$, H$_2$S, Ethenol, and LPG etc. at different operating temperatures. The pure film shows the response to H$_2$S gas at 300 °C for 100 ppm gas level while surface modified film shows the response to H$_2$S gas at room temperature for 100ppm gas level. The selectivity, Response and recovery time are the main characteristics of film were measured.

10. **To study the structural and electrical properties of n-type Cadmium selenide (Cd$_{1-x}$Se$_x$) thin films.**

**S. R. Vishwakarma, Aneet Kumar Verma, Ravishankar Nath Tripathi, Rahul and Sanjeev Kumar Maurya**

Department of Physics & Electronics,
Dr.R.M.L. Avadh University Fzd. (U.P.) India
*E-mail : verma.aneet@gmail.com, dr.rsnt@gmail.com*

CdSe is an important compound semiconducting material for the development of various applications in solid state devices such as solar cells, high efficiency thin film transistors. In recent years major attention has been given to the investigation of electrical and structural properties for the improvement of performance of such devices and its applications. In present investigation we prepared n-type CdSe thin films on glass substrate using Cd (99.999%) and Se (99.999%) powder as source materials of various composition ratio (Cd/Se) were prepared by

dry powder reaction in vacuum better $10^{-4}$ torr, heated below their melting point and then deposited by electron beam evaporation technique under vacuum $10^{-5}$ torr at room temperature and studied the effect of composition ratio (Cd/Se) on structural(Grain size, lattice parameter), electrical properties (charge concentration, resistivity, hall mobility ) of n-type CdSe thin films.

**11.    Effect of composition ratio (In/Sb) on structural and electrical properties of n-type InSb thin films  by electron beam evaporation technique**

**S. R. Vishwakarma, Rahul, Ravishankar Nath Tripathi,
Aneet Kumar Verma and Sanjeev Kumar Maurya**

Department of Physics & Electronics,
Dr. R. M. L Avadh University,
Faizabad–224 001 (U.P), India
*E-mail : rhl.jaunpur@gmail.com,  srvfzb@rediffmail.com*

Indium antimonide (InSb) semiconductor thin films were grown under vacuum $10^{-5}$ torr in Vacuum coating unit using prepared Indium antimonide semiconductor as a source materials. Indium antimonide semiconductor prepared by using In (99.999%) & Sb (99.999%) powder as various composition, formula In1-xSbx.(where x is variable having value 0.28 to 0.4). X-ray diffraction studies of the starting compound semiconducting materials and their thin films to confirm the polycrystallinity and show preferential orientation along the (111), (220), (311), and (400) planes. The grain size 'D', Dislocation density 'Γ' and lattice parameter 'a' of compound semiconductor and thin films were evaluated with XRD data. The grain size increased from 3.4 Å to 4.089 Å and dislocation density were decreased with increase of composition ratio(In/Sb) in InSb thin films. Electrical resistivity of thin films evaluated. Hall measurements indicate that the films were n-type, having carrier concentration $=10^{13}$ cm$^{-3}$, Hall coefficient$=10^{6}$ cm$^3$/coulomb and Hall mobility (0.87-1.236) $\times$ $10^{3}$ cm$^2$/v.sec for the film thickness of 300 nm. It is observed that the carrier concentration, Hall coefficient and hall mobility increases with increasing of In/Sb ratio.

### 12. Machinability Studies of Ti-8Al-4V by Coated and Uncoated K20 Inserts

**S. Madhavan[1], T. Deepak Kumar[2] and R. S. Karthik[3]**

[1]Department of Mechanical Engineering,
College of Engg, Anna university, Chennai
[2]Executive Engg Trainee,
L&T India Private Ltd, Chennai
[3]Department of Mechanical Engineering,
Sri Venkateswara College of Engineering,
Sriperumbudur, Chennai, Tamilnadu, India
[1]E-mail : madhavan.tes@gmail.com, Ph : 9941433180

Application of titanium alloy has increased many fields since the past 50 years. The major drawback encountered during machining was difficult to cut and the formation of BUE (Built up Edge). This paper presents the tool wear and surface roughness study of Ti-8Al-4 with K20 Tantalum thin film hard coated and uncoated carbide insert at moderate speed with the application of coolant. Titanium alloy is highly refractory metal and machining titanium is challenging to the manufacturers Experiments were carried out at medium duty lathe. Application of coolant tends to improve tool life and minimize adhesion of the work material on the cutting tool during machining. Result provides some useful information.

### 13. First-principles study of the cubic perovskites SrMO3 (M=Ti and Zr)

**Gaurang Misra**

Department of physics, Agra college,
Dr. B.R. Ambedkar University, Agra

The transition metalm oxides form a large, rich and stillnot well understood class of compounds. These can have unusual and useful electronic and magnetic properties.Many of these properties strongly depend on materials defects like vacancies, dislocations, stacking faults and grain boundaries. These defects affect local oxygen bonding. The origin of many properties of transition metal oxides is not always clear, which is an important problem to attack in solid state physics. The difficulty arises from the fact that the valence electrons in these materials have a strong mutual interaction. First-principles density- functional calculations are performed within the generalized gradient approximation to study the electronic properties of $SrZrO_3$, an insulating 4d perovskite, in the high-tempaterure cubic phase, above 1400 K, as

well as the generic 3d perovskite $SrTiO_3$, which is also a $d^0$ insulator and cubic above 105 K. The equilibrium lattice constant, bulk modules, first and second pressure derivatives of the bulk modules are obtained. The result are discussed also in terms of the exiting data in the literature for both oxides.

### 14. Analysis of Anderson-Gruneisen Parameter Under High Temperature

**Seema Gupta[1], Vipra Pandey[2], D. S. Tomar[3] and S. C. Goyal[1,3,4]**

Department of Physics, Agra College,
Agra–282 002
*Deptt. of Physics, B.S.A. College, Mathura
** R.B.S. College, Bichpuri, Agra
*** K.P. Engineering, College, N.H.-2, Agra

The Anderson Grüneisen parameter ($\Gamma$) is of considerable importance to Earth scientists because it sets limitations on the thermo elastic properties of the lower mantle and core. However, there are several formulations on the Grüneisen parameter which are in frequent use and predict varying dependence of ä as a function of temperature. In the present paper the expression for the thermal expansion, the thermal expansion coefficients and the bulk modulus are obtained considering the anharmonic dependence on temperature and is applied to study these constant to MgO. Using the derived expressions we have showed that different parameter on which Anderson Grüneisen parameter ($\Gamma$) depends are temperature dependent but over all Anderson Grüneisen parameter ($\Gamma$) is impendent of temperature. The result obtained is found to compare well with experimental data.

### 15.   Sn-doped TiO2 Thick Film Resistor as a Gas Sensor

**[*1]P. D. Hire, [2]V. B. Gaikwad, [3]N. U. Patil, [4]R. L. Patil and [5]G. H. Jain**

[1]Dept of Electronic Science, K.T.H.M. College,
Nasik–422 002, India
[2]Dept of Chemistry, K.T.H.M. College,
Nasik–422 002, India
[3]Dept of Physics, Arts, Science and Commerce College,
Igatpuri, India
[4]Dept of Physics, K.T.H.M. College,
Nasik–422 002, India
[5]Dept of Physics, Arts, Science and Commerce College,
Nandgaon, India
*\*E-mail : pdhdesrane@gmail.com*

Sn-doped TiO2 (ST) mixture was prepared by using mechanochemical process. As prepared ST was then used as starting material to fabricate the sensors in thick film form. Thick films were prepared by screen-printing technology on glass substrate. Dipping technique was used to modify surface of ST films. The characterization of the films was done by XRD and SEM. The gas response measurements were carried out as function of operating temperature for different gases. Pure ST films were observed to be highly sensitive to H2 gas at 250OC and surface modified by NiCl2 ST film showed response to Cl2 gas at 450OC.The result indicated that surface modification of films changes the adsorption-desorption relationship with target gas and shifts its selectivity.  The gas response, selectivity, response and recovery time of the pure and modified films were measured and presented.

### 16.   Psidium guajava leaf mediated biosynthesis of gold nanoparticles

**S. L. Smitha and K. G. Gopchandran**

*Department of  Optoelectronics,
University of Kerala,
Thiruvananthapuram–695 581, India*

Biological synthesis of gold nanoparticles by the reduction of aqueous chloroaurate ions using Psidium guajava leaf broth as the reducing agent is reported. The effect of leaf broth concentration and pH value of the reaction solution on the formation of Au nanoparticles ware also investigated. The morphology of the particles formed consist of a mixture of triangular and

spherical particles and with increase in concentration of leaf broth, spherical particles dominates. Good crystallinity of the nanoparticles with fcc phase is evident from XRD patterns, clear lattice fringes in the high resolution TEM image and bright spots in the SAED pattern. Small spherical particles of size $\sim$ 4 nm were formed at a pH of 10.5, while large particles of size $\sim$ 4nm were formed at a pH of 10.5, while large particles of size $\sim$ 25 nm are formed at a pH of 1.

**17. Study of Layer Transfer Approaches on Thin film Crystalline Silicon Solar Photovoltaic Cells**

**Vimal Sagar, Sunit Kumar[*] Anita Sagar[**], Ramdeo Yadav[***] and A. P. Yadav[****]**

P.G.Department of Physics,
B.N. Mandal University,
Madhepura, Bihar
*Department of Statistics,
Jamshedpur Co-Operative College,
Jamshedpur
**Department of Computer Science,
Jamshedpur Womens College, Jamshedpur.
*** Department of Physics, G.B.College,
Naugachia, Bhagalpur, Bihar
****Department of Physics, Marwari College,
Darbhanga, Bihar
*E-mail : dr.vimalsagar@yahoo.co.in*

CdTe Solar Photovoltaic Cells are facing obstacle in production due to the toxicity of Cd. For these reasons, Crystalline Silicon Cell will continue to play a dominant role in Solar Photovoltaic Cells market. Thin film Crystalline Silicon Solar Photovoltaic Cell have an active layer thickness of several microns to tens of microns, have been of considerable interest for Research & Development. The mechanism for enhancement of efficiencies of Thin film Crystalline-Silicon Solar photovoltaic cells requires the detachment of Silicon films from a single Crystal Substrates. These new techniques promise higher efficiencies of Crystalline Silicon Solar photovoltaic Cells than the more traditional Thin film Poly-Crystalline Silicon Solar Photovoltaic Cells.

In this paper we study the advantages of layer transfer approaches on Thin film Crystalline Silicon Solar Photovoltaic Cell.

### 18. Microstructural and compositional properties of co-sputtered Ni-Ti shape memory alloy thin films

**B. Geetha Priyadarshini [1], S. Aich[1] and M. Chakraborty[1,2]**

[1]Department of Metallurgical and Materials Engineering,
Indian Institute of Technology,
Kharagpur–721 302, India
[2]School of Mechanical Sciences,
Indian Institute of Technology,
Bhubaneswar–751 013, Orissa, India

The present report discusses about the microstructural and compositional properties of co-sputter deposited NiTi films on Si (100) upon variation in the substrate conditions. The associated microstructure was explored by Field Emission Scanning Electron Microscope (FESEM) and High Resolution Transmission Electron Microscope techniques (HRTEM). High substrate temperature was found to influence the morphology of the Ni-rich NiTi films leading to the formation of bimodal grain size distribution without affecting the composition of the films. Further, TEM micrographs and electron diffraction studies revealed the co-existence of crystalline and amorphous phase in deposited Ni-rich NiTi film. Application of bias voltage of -100 V to the substrate during deposition of Ti-rich NiTi films lead to the nanocrystalline films with smooth, compact texture. Attempts are made to discuss the possible mechanisms behind the evolution of such microstructures in NiTi thin films.

### 19. AFM and Resistivity Studies in Ni/Fe Multilayers

**[a]P. J. Sadashivaiah, [a]T. Sankarappa*, [b]T. Sujatha, [a]Santoshkumar**
**[c]R. Rawat and [d]A. K. Bhatnagar**

[a]Department of Physics, Gulbarga University,
Gulbarga–585 106, Karnataka, India
[b]HPS, Kalkhora, Basavakalyan (Tq), Bidar (Dt),
Karnataka, India
[c]UGC-DAE Consortium for Scientific Research,
Indor–452 001, India
[d]School of Physics, Hyderabad University,
Hyderabad, India
*E-mail : sankarappa@rediffmail.com*

The multilayers, $[Ni(100nm)/Fe(100nm)]_n$; n = 1,2,3 and 5 were deposited at 200 °C

using electron beam gun method and investigated for structure and electrical resistivity variation with temperature in the range from 4.2K to 300K. The grain size and surface roughness were determined by atomic force microscope (AFM). The residual resistivity ratio (RRR) and the temperature coefficient of resistivity (TCR) were determined. The power law exponents for the resistivity variation with temperature have been determined by regressional analysis. The power law exponent was close to unity for temperature above 80K and was between 3 and 5 for temperature below 30K. The contribution to resistivity for temperature above 80K is attributed to the domination of electron-phonon scattering and for below 30K it is dominated by electron-electron and electron-defect scattering besides some contribution from the electron-magnon scattering. It is for the first time Ni/Fe multilayers in the present configurations were investigated for surface morpology and electrical resistivity and power laws for the resistivity variation with temperature in the range from 4.2K to 300K have been determined.

## 20.   Dielectric and Alternating conductivity in $Fe_2O_3$ and $B_2O_3$ doped Phosphate Glasses

**B. Vijaya kumar[a], S. S. Veena[b] , T. Sankarappa[a*], T. Sujatha[c] and P. J. Sadashivaiah[a]**

[a]Department of Physics, Gulbarga University,
Gulbarga, Karnataka, India
[b]Department of Physics, RBYM Engineering College,
Bellary, Karnataka, India
[c]HPS,Kalkhora, Basavakalyan (Tq),
Bidar (Dist), Karnataka, India
*E-mail : sankarappa@rediffmail.com*

A series of phosphate glasses in the compositions, $(B_2O_3)_{0.10}$-$(P_2O_5)_{0.9-x}$-$(Fe_2O_3)_x, 0.1 \xi x \nleq 0.4$ have been prepared by melt quenching method and investigated for dielectric properties and conductivity in the frequency range from 100Hz to 5MHz and temperature range from 325K to 550K. From the total conductivity the frequency exponent, $s$, dc and ac components of the conductivity were determined. Both dc and ac conductivity increased with $Fe_2O_3$ content and temperature. Mott's small polaron hopping model has been invoked to understand the temperature dependence of both dc and ac conductivities and their activation energies have been determined. DC activation energy decreased with $Fe_2O_3$ content. Ac activation energy also decreased with $Fe_2O_3$ content and frequency. Variation of both ac and dc conductivity and their activation energies with $Fe_2O_3$ indicate that the number of polarons are increased and the spacing between TMI sites decreased with the addition of $Fe_2O_3$. It is for the first time that

$Fe_2O_3$ and $B_2O_3$ doped phosphate glasses have been investigated for dielectric properties and conductivity over wide temperature and frequency ranges and the data analyzed.

**21.  Examination of process parameter combination to achive good surface finish in machining at a moderate cutting speed using taguchi analysis**

**T. Rajasekaran[1A], K. Palanikumar[B] and B. K. Vinayagam[A]**

[A]School of Mechanical Engineering, SRM University,
Kattankulathur–603 203, Tamilnadu, India
[B] Sri Sairam Institute of Technology,
Chennai–600 044, Tamilnadu, India
*E-mail : rajasekaran@ktr.srmuniv.ac.in,   rajasekaran2k@yahoo.com*

One of the important interests in the machining is attaining better surface roughness as well as dimensional accuracy. Fiber reinforced polymer composite materials are the one which are produced near to the required shape, further machining is necessary to achieve expected surface characteristics. This experimental study targets the machining of carbon fiber reinforced polymer material made into the form of tube. It examines various process parameters such as cutting speed, feed and depth of cut and their importance in deciding the  surface roughness. Taguchi's concepts such as orthogonal array and ANOVA were used to analyze the process parameters.

**22.  Computer Simulation Study of Schottky Vacancy Formation Energy of Ionic Solids**

**B. Srinivasa Rao\*, S. Jagadeesh Babu\*, N. Radhika\*\*,
S. D. V. Prasad\* and S. P. Sanyal^**

\*Department of Computer Science and Engineering,
Malla Reddy Engineering College,
Maisammaguda, Medchal(M), Hyderabad–500 014
\*\*Department of Physics, Malla Reddy Engineering College for Women,
Maisammaguda, Medchal (M), Hyderabad–500 014
[+]Department of Physics, University of Bhopal,
Bhopal, India–462 026

The Computer Simulation Studies have been playing a significant role in understanding the structural, mechanical, and electrical properties of the crystalline solids over the last few

decades. It is well known that Schottky defects play significant role in the physical properties such as diffusion, ion transport and mechanical properties of the ionic crystals. Literature revels that the schottky defect energies calculated using two body potentials and polarizable point ion model have not included the overlapping charges. Also the polarizabilites used in these calculations were derived arbitrarily. In order to overcome these limitations, in the present work we propose a three body potential that include three body interactions due to overlapping charges in both perfect and defect lattice. In the present paper we report calculated values of formation energies ($h_{vp}$) and binding energies ($h_B$) of Schottky defects in some ionic crystals such as NaCl, KCl, NiO and CoO. For NaCl $h_{vp}$ = 1.30ev and $h_B$ =1.37ev; for KCl $h_{vp}$ = 1.42ev and $h_B$ = 1.36ev; for NiO $h_v$ = 6.06ev; and for CoO $h_v$ = 6.81ev. The comparison of the results reveal that the calculated values of schottky defect formation energies for these ionic solids have a good agreement with the corresponding experimental values and they are better than the previous theoretical results. In conclusion, the agreement achieved between the present theoretical results and available experimental data emphasizes the contribution of the TBI effect to the polarization in the defect region.

### 23.  Dielectric properties of nanotitania tubes synthesized by low temperature hydrothermal method

**Abdul Gafoor A. K.[a], M. M. Musthafa[a] and P. P. Pradyumnan[a*]**

[a]Department of Physics,
University of Calicut,
Kerala–673 635, India

Nanotitania tubes in pure anatase phase were prepared by low temperature hydrothermal method. The X-ray diffraction analysis confirmed that the samples have pure anatase phase. The average tubular size of the prepared sample is 100 nm. The synthesized nanotitania tubes were characterized using X-ray diffraction (XRD), Energy Dispersive X-ray Spectroscopy (EDX) and Scanning electron microscopy (SEM). Dielectric properties of nanotitania tubes were studied as a function of the frequency of the applied ac signal at different temperatures in the frequency range of 42 Hz to 5 MHz. It was observed that the real dielectric constant H′ is extremely high of the order $10^4$ in the low frequency region. The loss spectra obtained at various temperatures are characterized by peaks appearing at the frequency 1 KHz suggest the existence of relaxing dipoles in the sample. As the frequency of applied field is increased, dielectric constant and

dielectric loss are decreased. This property of the material could be used to fabricate energy storage devices, more reliable super capacitance DRAMs cell and high density DRAMs.

## 24. Synthesis and Characterization of Colloidal CdSe NRs, NBs and CdSe/ZnS Quantum Dots

**G. Ramalingam, J. Madhavan and P. Sagayaraj**

Department of Physics, Loyola College,
Chennai–600 034, India

Large scale, uniform and well-dispersed CdSe nanorods(NRs), nanobelts(NBs) and CdSe/ZnS Quantum dots (QDs) were successfully synthesized via solvothermal routes. CdSe nanorods with a mean diameter and length of 25 nm and 82 nm respectively are synthesized and the problem of handling the stacking faults present in the long CdSe nanorods is analyzed. The CdSe/ZnS QDs are monodispersive of 4-7 nm diameters. The nanostructures were characterized by powder x-ray diffraction (XRD), transmission electron microscope (TEM/HRTEM) and energy dispersive x-ray analysis (EDAX). The effect of experimental parameters on the formation of different morphology and possible growth mechanism were investigated. The studies on the optical properties CdSe NRs, NBs and QDs were carried out by UV-Vis absorption spectrum and photoluminescence (PL) spectrum.

## 25. Electrical and Structural Characteristics of CdS Thick films Fired in RTP Furnace

**S. C. Karle[1, 2] and A. D. Shaligram [2]**

[1]Department of physics, New Arts,
Commerce & Science College,
Ahmednagar, Dist : Ahmednagar–414 502, India
[2]Department of Electronic Science,
University of Pune,
Pune–411 007, India

The CdS films fabricated using thick film technology and fired in RTP farness are characterized by different techniques. The electrical properties of CdS thick films are measured using Rish-Multi-15S with memory Adopter SI-232. This technique shows decrease in resistance of the devices with intensity of illumination. The results are compared with commercial CdS

photoconductors which shows dark resistance of the order of $10^6$ ohm Specimen to specimen variability in terms of dark resistance is 0.4 to 1.34 Mhom and sensitivity is 2.5 to 7.52 ohm/ w is observed. The structural properties are also studied using Microscope. It shows microstructure and morphology of the CdS thick films.

### 26.   Thermo-Physical Properties of Nano-$TiO_2$ Dispersed ethylene glycol based nanofluids

**Gayatri Paul[1], P. K. Das[2] and I. Manna[1,3]**

[1]Department of Metallurgical and Materials Engineering,
IIT Kharagpur–721 302, WB
[1]Department of Mechanical Engineering,
IIT Kharagpur–721 302, WB
[1]Central Glass and Ceramic Research Institute (CSIR),
Jadavpur–700 032, WB
*E-mail : gayatri.paul@gmail.com*

Thermal conductivity and viscosity of nano-$TiO_2$ dispersed ethylene glycol based nanofluids (prepared by two-stage process) have been measured using a transient hot wire device and parallel plate type rheometer, respectively. The thermal conductivity of the nanofluids is observed to be strongly dependent on factors like concentration of dispersed nanoparticles, ambient temperature and time interval between successive measurements. A maximum thermal conductivity enhancement of 20% has been observed at a concentration of and 0.1 vol% of dispersed nanoparticles. Temperature has a strong influence on thermal conductivity of nanofluids as thermal conductivity at 70°C increases by more than 100% with respect to that of ethylene glycol at 70°C. However, the nanofluids exhibit an unusual behavior with viscosity at all concentrations of dispersed nanoparticles being lower than that of base fluid under the same experimental conditions. Though Newtonian flow behavior is followed by nanofluids at all concentrations, the lowered viscosity compared to that of base fluid is a unique behavior and the plausible cause for such a behavior will be discussed in the talk.

### 27. Magnetic susceptibility measurements on Fly ash admixtured cement

**R. Gopalakrishnan**

Department of Physics, SRM University,
SRM Nagar–603 203, Tamilnadu, India
*E-mail : rgopal_ra@rediffmail.com*

The present works reports the effect of Fly ash on the properties of Portland cement hydrated with distilled water through magnetic susceptibility study. Cement pastes containing 0, 10, 20, 30% replacement of fly ash with cement and in a W/C ratio of 0.4 have been prepared. The magnetic susceptibility at different hydration ages has been determined by Faraday Curie balance method and this has been related to changes in setting time and compressive strength measurement. The observed result shows that, the magnetic susceptibility values increases with increasing fly ash percentage replacement level in cement.

### 28. Morphological and compressive strength studies on metakaolin admixtured cement

**R. Gopalakrishnan**

Department of Physics, SRM University,
SRM Nagar–603 203, Tamilnadu, India
*E-mail : rgopal_ra@rediffmail.com*

The hydration reaction, morphology of cement paste with part of Portland cement replaced by metakaolin were investigated by Compressive strength and Scanning electron microscopy studies. The results shown that the replacement of Portland cement by metakaolin can decrease the amount of $Ca(OH)_2$, increase the amount of C-S-H gel, make the structure denser, improve the cementitious properties and compressive strength of cement paste.

### 29. High Pressure Phase Transition of Scandium Arsenide

**Purvee Bhardwaj and Sadhna Singh**

High pressure Physics Lab.,
Department of Physics,
Barkatullah University,
Bhopal–462 026, India
*E-mail : purveebhardwaj@gmail.com*

In the present paper, we have investigated the high-pressure structural phase transition of scandium arsenide (ScAs). We have used the three body interaction potential model to calculate the phase transition pressure. Phase transition pressures are associated with a sudden collapse in volume. At compressed volumes, this compound is found CsCl phase. The phase transition pressures and associated volume collapses obtained from present potential model show a generally good agreement with available experimental data than others.

### 30. Optical and electrical properties Ge quantum-dots on Si (001) substrate grown by molecular beam epitaxy

**R. K. Singha, S. Das, S. Manna, A. Dhar and S. K. Ray**[*]

Department of Physics and Meteorology
Indian Institute of Technology,
Kharagpur–721 302
*\*E-mail : physkr@phy.iitkgp.ernet.in*

Self-assembled $Ge_xSi_{1-x}$ islands were grown on Si (001) substrates by solid source molecular beam epitaxy (MBE). The growth of different morphological shapes and sizes were controlled by tuning the growth parameters. Micro Raman analysis, HRXRD and surface analytical tools (AFM, FESEM, TEM) were routinely used to investigate the composition, intermixing and strain of resultant islands. The observed infra-red photoluminescence signal from grown samples was associated with radiative recombination of holes confined in the Ge islands and electrons localized in the Si buffer layer. The grown samples showed noble room temperature far IR photocurrent response that can be used as key tools for optical communication and monolithic integration with present CMOS technology. The self-assembled Ge/Si quantum dots showed unique electrical properties such as low dark current compared to present reported results. The single quantum dot shows stair case like I-V characteristics investigated through conducting

atomic force microscopy (CAFM). The grown Ge quantum dot is a promising candidate for futuristic single hole transistor for low power faster operation.

### 31.    Physical Properties of ternary Semiconductors-Few Alloys

**SriVani. Gurram Research Scholar**

Rayalaseema University
Kurnool District, A.P, India
*E-mail : Raghava_gurram@rediff.com*

The world of physics has been completing hundreds of years in applying scientific methodologies to understand basic principles of nature, matter and energy and how they interact. A Physicist means one who studies and makes research within one area of physics through interaction with many other disciplines. There are many subjects of physics from very small particle physics to very large cosmology or study of the Universe. In these vast areas of subjects Semiconductor technology plays a vital role.

The optical and related properties of few II-VI semiconductors are studied in the design and analysis of Opto-electronic devices. Various analytical expressions were developed to study the optical constants of refractive index, band energy gap, and absorption coefficient. These are used to evaluate variation of refractive index with pressure (dn/dp) and effective mass of charge carriers in ternary semiconductors and comparison of the results is made with available reported values.

### 32.    Microwave Assisted Synthesis of Mushroom Like Nanofibers ZnO – SnO$_2$

**R. Kannan[a], A. Obadiah[a], A. Ramasubbu[b] and S. Vasanthkumar[a*]**

[a]Department of Chemistry,
School of Science and Humanities,
Karunya University,
Coimbatore–641 114
[b]Department of Chemistry,
Govt. Arts College (Autonomous),
Coimbatore–641 018

The novel properties of nano – materials depend on their size and shape/Morphology of

nano structured materials are key issues in nano–material science. Zinc and tin oxides have recently attracted considerable attention because they exhibit interesting technological properties. Tin oxide based materials find extensive application in a various fields like sensor, micro and nano electronic devices, and flat panel displays. Recently, conductive oxides such as Zinc and tin, have been found to high electron mobility, electrical conductivity, thermal durability and better properties than ZnO and $SnO_2$ alone. $ZnO–SnO_2$ based materials are potential material for conductive transparent glasses in solar cell fabrications and gas sensors. In order to get nano fibers of $ZnO–SnO_2$ various processing routes, including conventional high temperature solid–state reaction between $SnO_2$ and ZnO, spray pyrolysis, sol-gel, mechanochemical and chemical coprecipitation method have been tried and reported. However, these methods are expensive for the production of commercial nano oxides and are also complicated synthetic routes. Herein, we reported the facile strategy for the bulk synthesis of $ZnO–SnO_2$, with high porous structure in a short span of time. The results are discussed in detailed.

### 33.    Amorphous MoN films as a diffusion barrier for copper metallization

**Anuj Kumar, Mukesh Kumar and Dinesh Kumar\***

Electronic Science Department,
Kurukshetra University,
Kurukshetra–136 119, India

The barrier capability of 50 nm thick amorphous MoN thin film was investigated against Cu diffusion. MoN layers were deposited using reactive sputtering technique at different nitrogen flow rates. The characterization of the samples was carried out using X-ray diffractometer (XRD), four probe method and scanning electron microscope (SEM). Results indicate that the amorphous MoN layer has been successfully deposited and has been found to act as a good diffusion barrier upto 600 °C.

### 34. Band gap modulation in ZnCdO thin films deposited by Sol-Gel method

**Amanpal Singh, P. K. Khanna and Dinesh Kumar***

Electronic Science Department,
Kurukshetra University,
Kurukshetra (Haryana)–136 119
Central Electronics Engineering Research Institute,
Pilani (Rajastahn)–333 031

The nanocrystalline crack free thin films of cadmium doped zinc oxide have been deposited on corning 7059 glass by sol-gel process. The sol with different concentration of cadmium is prepared using hydrate zinc acetate precursor and 2-methoxyethanol solvent with ethanolamine as a sol-stabilizer. The annealing temperature is optimized by annealing at different temperatures of $Zn_{1-Y}Cd_YO$ keeping the concentration constant (Y$=0.10$) thin film. The doping of cadmium was confirmed by X-ray diffraction. An increase in the cadmium content leads to crystallinity degradation and the (002) peak shifted to lower angle. The energy band gap is determined from UV-Vis spectroscopy. The energy band gap of ZnCdO thin films decrease with increasing Cd content.

### 35. Study of structural, optical and electrical properties of $SnO_2$–ZnO composite thin films prepared through pulsed laser deposition

**S. K. Sinha[1], T. Rakshit[2], S. K. Ray[2] and I. Manna[3]**

[1]Metallurgical and Materials Engineering Department,
Indian Institute of Technology,
Kharagpur–721 302, India
[2]Physics and Meteorology Department,
Indian Institute of Technology,
Kharagpur–721 302, India
[3]Central Glass and Ceramic Research Institute,
Kolkata–700 032, India

In this work, the effect of ZnO as bulk dopant in electrical, structural and optical properties of $SnO_2$ thin films prepared through pulsed laser deposition technique.

Zinc oxide, in five different concentrations (1 wt%, 5 wt%, 10 wt%, 25 wt% and 50 wt%) was doped with $SnO_2$. The films were deposited on Si (100) substrates under positive oxygen environment at 500 °C temperature. The AFM analysis of the films shows that the RMS

and average surface roughness ($R_a$) value decreases with increasing ZnO content. The composite ZnO-$SnO_2$ films shows amorphous behavior at higher ZnO concentration ($>10$ wt%), as evident from the GIXRD patterns. The resistivity of the composite samples increases with increasing ZnO concentration (beyond 10 wt% ZnO). Absorbance spectra were taken to examine the optical properties, and the composite samples shows a noticeable increase in band gap energy compared to either pure ZnO or pure $SnO_2$ films.

### 36. Isothermal oxidation kinetics of nano-$Y_2O_3$ dispersed ferritic steel developed by mechanical alloying and hot isostatic pressing

**S. K. Karak[1], A. Meherwal[1], W. Lojkowski[2], J. Dutta Majumdar[1] and I. Manna[1,3]**

[1]Metallurgical and Materials Engineering Department,
Indian Institute of Technology,
Kharagpur–721 302, India
[2]Institute of High Pressure Physics (Unipress),
Polish Academy of Sciences,
Sokolowska 29, 01-142 Warsaw, Poland
[3]Central Glass and Ceramic Research Institute,
CSIR, 196 Raja S. C. Mullick Road,
Kolkata–700 032, India

Oxidation kinetics of high Cr ferritic steel, synthesized by mechanical alloying of elemental powder blend 1.0 wt % nano-$Y_2O_3$ dispersed 83.0Fe-13.5Cr-2.0Al-0.5Ti (alloy A), 79.0Fe-17.5Cr-2.0Al-0.5Ti (alloy B), 75.0Fe-21.5Cr-2.0Al-0.5Ti (alloy C), and 71.0Fe-25.5Cr-2.0Al-0.5Ti (alloy D) alloys (all in wt %) and subsequent consolidation of the milled powder by hot isostatic pressing (HIP) at 1000 °C using 1.2 GPa uniaxial pressure for 1.0 h have been studied under isothermal (700 – 900 °C for up to 50 h) conditions in dry and still air. Evolution of microstructure and phase aggregate of milled powders during mechanical alloying and or oxide scale following isothermal or non-isothermal oxidation were studied using scanning electron microscopy, energy dispersive X-ray spectroscopy, X-ray diffraction. Oxidation mostly occurred by counter-ionic transport of oxygen from ambience to the core and cations ($Cr^{+3}/Fe^{+3}$) from the core to the surface predominately through grain boundaries at low temperature ($\sim 600$ °C) and through grain bodies at high temperature ($\sim 700 – 900$ °C). Early segregation of Cr to ferritic grain boundaries and promotes formation of Cr-rich spinel layers along the boundaries near the surface and prevents further oxidation or scale growth.

**37.** **Comparison of the Conventional sub-zero temperature treatments and cryogenic treatments of materials. A review of Literature**

**K. Shanmugam**

Professor, School of Mechanical Engineering,
SRM University,
Kattankulathur–603 203

The use of sub-zero temperature treatment as an integral part of heat treatment is not a recent development. Extensive use of such treatments has been made for many years on case hardening of steels such as En36 and En 39 following hardening and also in the aircraft industry

Conventional sub-zero treatments have been carried out at temperature of approximately –80 $^{\circ}$C. Many authorities express that this is sufficient to fully transform austenite retained in the quenched microstructure. However, more recent evidence has shown that beneficial effects of tool life are enhanced by treatment at even lower temperature such as those generated by liquid nitrogen at –196 $^{\circ}$C.

For many years, the value of cryogenic treatment of steel and other materials has been debated. Even today many metallurgical professionals have serious reservations about its value. Notwithstanding these concerns, it is the intent of this discussion to review some of the current literature and practices of those who believe that cryogenic treatment enhances steel properties than sub-zero treatment.

**38.** **Influence of waters on early hydration of fly ash-blended cement**

[a]*****Thiruppathl. K** and [b]**Barathan. S**

[a]Valliammai Engineering  College,
Srm Nagar, Kattankulathur
[b]Annamalai University,
Annamalai Nagar, Chidambaram
*E-mail : thiruraj_ka@rediffmail.com*

In this paper, investigations were undertaken to formulate the properties of fly ash-type V Cement matrix by blending fly ash with type V (CSA) cement. The effects of the quality of mixing water and initial hydration of cement were investigated by considering different levels

of fly ash replacement. Fly ash was used as a partial replacement of type V Portland cement at 0%, 5%, 10%, 15%, 20%, 25%, 30% and 50% by weight. Water to binder ratios ( $W/B$ ) were varied at 0.4, 0.45, and 0.5 for different waters. The pore structure, early hydration phases, and reaction behaviour of heavy metals Zn and Pb for fly ash-type V cement matrices were determined by dielectric and conductivity and compared with setting time. The results showed that the addition of fly ash to form fly ash-type V cement matrix reduced the setting time compared to that of pure type V cement matrix. However, fly ash-type V cement matrix could effectively immobilize high concentration of heavy metal such as lead and zinc. Besides ettringite AFt, Friedel phase was a new hydration phase formed in the matrix. The formation of these hydration phases was responsible for huge reservoir of heavy metal stabilization by chemical fixing. The use of a higher water-to-binder ratio for the preparation of cement containing fly ash paste has a greater effect on the composition of the hydrate assemblage, while it significantly changes the composition of the pore solution. Among the addition of fly ash with cement, 30% was the optimum percentage.

## 39.　Effect of Concentration on Physical Properties of few III-V Ternary Compounds

**V. Rama Murthy and Alla. Srivani**

P.G Department of Physics,
T.J.P.S College Guntur-6 A.P India

Characterization of Semiconductors is very important as an x of a constituent in the Semiconductor is going to have significant changes in calculating physical properties of ternary compounds. The subscript X refers to the alloy content or concentration of the material. The compositional dependence of physical properties with the % of the constituent exhibits linear variation. The Linear variation or the presence of nonlinear increments in the Physical property with the change in value of x, the % of the constituents is also a factor. In the large family of ternary compounds one could expect to find systematic trends for the various physical properties. For instance the geometrical arrangement of the atoms is in most ternaries, tetrahedral.

**40. Thermal, optical, mechanical and dielectric properties of non linear optical material 4 Methoxy benzaldehyde -n-methyl 4-stilbazolium tosylate**

**Amirdha Sher Gill and S. Kalainathan**

School of Advanced Sciences,
VIT University, Vellore,
Tamil Nadu–632 014, India

We have grown organic non-linear optical 4-methoxy benzaldehyde - N -methyl - 4 - stilbazolium tosylate crystals by slow evaporation technique. The grown crystals were analyzed by powder XRD, FTIR, NMR, UV, Thermal, mechanical and dielectric measurements. Lattice parameters and crystallinity of the crystal is confirmed by the XRD studies. The FTIR and NMR studies give the details about the various functional groups present. In order to study the optical quality of the crystal, the UV-vis absorption spectrum was recorded and cut-off wavelength was determined. Melting point of the crystal is found from the differential scanning calorimetry. The powder SHG studies were done with Kurtz powder technique and the NLO efficiency is 17.2 times greater than urea.

**41. Graft Co- Polymerization of casein with poly Methyl Methacrylate and Incorporation of chitosan containing silver Nanoparticles**

**K. Mohammed Farhan[1], N. V. Nishitha[1], Y. Lakshminarayana[2],
M. Pandima Devi[3], T. P. Sastry*[1] and A. B. Mandal**[4]**

[1]Bioproducts laboratory,
Central Leather Research Institute, Adyar,
Chennai–600 020
[2]Polymer Division,
Central Leather Research Institute, Adyar,
Chennai–600 020
[3]Department of Biotechnology,
School of Bioengineering,
SRM University, Kattankulathur–603 203
[4]Director, Central Leather Research Institute,
Council of Scientific and Industrial Research, Adyar,
Chennai–600 020
*E-mail : *sastrytp@hotmail.com, **abmandal@hotmail.com*

Fabrication of nanomachines, nanoelectronics and other nanocomposites will undoubtedly solve an enormous amount of the problems faced by mankind today. In the present study we

have prepared a nanocomposite containing casein-co-polymethyl methacrylate and incorporation of chitosan containing silver nanoparticles. Tensile strength, Infrared Spectroscopy, Thermogravemetric analysis, Scanning Electron Microscopy and conducting studies were carried out using the samples prepared. Casein graft co-polymer (c-g-PMMA) has shown better mechanical properties than the control film. The Infrared Spectrum proved the grafting of poly methylmethycrylate (PMMA) on the casein. The Thermogravemetric studies have shown that the graft co- polymer was thermally stable up to 450 °C compared to casein film. The Scanning Electron Microscope studies have shown orderly arrangement of silver nanoparticles on the surface of casein graft co – polymer impregnated with silver nanoparticles (c-g-PMMA-AgNP). (cg-PMMA-AgNP) has shown electric conductivity of 7 to 17 mega ohms. This product may be useful in the future for the preparation of conducting polymers.

### 42.   A Laser effects induced optical phonon modes of Raman study for nanostructured In doped ZnO thin film (In : ZnO)

**G. Kavitha[*], P. Babu[1], R. Krishnan[3], E. Manikandan[2,3],**
**V. John Kennedy[4], B. K. Panigrahi[3] and K. G. M. Nair[3]**

[1] P.G and Research Dept of Physics,
A.M. Jain College, Meenambakkam,
Chennai–600 114, India
[2]DST/CSIR Nanotechnology Innovation centre, NCNSM,
Council for Scientific and Industrial Research (CSIR), Pretoria 0001,
Republic of South Africa (RSA)
[3]MSG, Indira Gandhi Centre for Atomic Research (IGCAR),
Kalpakkam–603 102, Tamilnadu, India
[4]Ion Beam Physics & Nanotechnology, National Isotope Centre,
GNS Science (Institute of Geological & Nuclear Sciences),
Wellington, New Zealand

The nanostructured ZnO and In doped ZnO thinfilm were prepared by p-Si(100) substrates by pulsed laser deposition at 300C in the inert Ar gas atmosphere . The synthesised films were characterized by X-ray diffraction, micro-Raman scattering field emission scanning microscope for structural, optical and surface morphology and photoluminescence spectroscopy at room temperature. In this present study, we mainly devoted for finger print technique of Raman optical phonon mode intensity difference with the incident laser wavelength 514.5 nm [E$=$2.405 eV, argon ion (Ar$^+$)] power variably. The Raman spectra of ZnO and doped films shown the

characteristic wurtzite phase has assigned at 438 cm$^{-1}$ $E_2$ (High). This indicates that the wurtzite structure formed, ZnO and In : ZnO crystal quality phase is good, which is agrees with X-ray results. The Raman spectrum shows the wurtzite phase $E_2$ higher intensity peaks at lower incident laser power 438 cm$^{-1}$. When the increasing the laser power onto the samples and decreasing the intensity of the characteristic peak in both samples. Similarly, the peak shift toward to bathochromic shift $E_2$ resonance mode at 98 cm$^{-1}$ is due to the nanoscale particle size of the deposited ZnO compared to the bulk. A similar shift difference in the $E_2$ (non-polar phonon) resonance mode compared to bulk ZnO is reported for ZnO nanobelts obtained via evaporation of ZnO powder. Due to incorporation of In the small peak might be appear in the nanostructured films. This attribute that the extrinsic dopant of Indium and the raising incident laser heat such as local temperature effect on the band gap shift also discussed.

## 43. Styrene Butadiene Rubber-Organically Modified Clay Nanocomposites- Effect of Processing conditions on the Mechanical, Morphological and Rheological properties

**K. S. Usha Devi and Dr. Sabu Thomas**

Department of Chemistry,
N.S.S. College, Pandalam
Professor, School of Chemical Sciences,
M.G. University, Kottayam

The recognition of the unique properties of polymer nanocomposites has a great significance in material chemistry. Nanocomposites with different weights of Organically Modified Clay were prepared using the SBR matrix and Sulphur cure package. Samples were prepared by swelling clay in toluene, mixing with polymer in solvent and by traditional mill mixing method. A gum sample without adding any clay was also prepared. The samples were subjected to Mechanical and XRD analysis. The morphology of the specimen was analyzed by Scanning Electron Microscopy (SEM) and Transmission Electron Microscopy (TEM). Rheology was used to find out the extent of polymer filler interaction. The mechanical strength of the samples was compared.

### 44.    One-pot synthesis of semiconducting PbS nanorods and nanocube within polyphenylene sulphide matrix

**Sujata Kasabe[1*], Parag Adhyapak[2], Manish Shinde[2], Uttam Mulik[2] and Dinesh Amalnerkar[2*]**

[1]Abasaheb Garware College, Karve Road,
Pune–411 004, India
[2]Center for Materials for Electronics Technology,
Panchawati, Off Pashan Road,
Pune–411 008, India
*E-mail : smw1_06@yahoo.co.in*

Herein we report one-pot in-situ preparation of lead sulphide nanorods and nanocubes inside polyphenylene sulphide matrix. The PPS plays a dual role in the synthesis; it acts as a chalcogen source as well as provides a stabilizing matrix for the resultant nanorods. The process is very simple and cost effective. The effect of molar ratios of the reactants on the morphology of the nanorods was studied. The prima facie observations suggest the effective formation of lead sulphide nanorods along with nanocube (rock salt type) structure with 25 nm size.

### 45.    Controlling the Nanoparticle Size and Enhanced Gas Sensing Properties of $SnO_2$

**Muthuvinayagam A[a]. Boben Thomas[b],   N. Melikechi[c] and Sagayaraj P[a]**

[a]Reseach Centre in Physics,
Loyola College, Chennai,
Tamil Nadu–600 034, India
[b]Reseach Centre in Physics,
Mar Athanasius College, Kothamangalam,
Kerala–686 666, India
[c]Centre for Research and Education in Optical Sciences and Applications,
Department of Physics and Pre –Engineering,
Delaware State University,
Dover DE 19901, US

The emerging nanoscience and nanotechnology stimulate extensive research on nanostructured metal oxides has found potential or practical applications in various types of solid state gas sensors. Tin dioxide ($SnO_2$) is an important n-type wide-energy-gap semiconductor ($E_g = 3.6$ eV, 330 K) which has a broad range of gas sensor applications. It has been demonstrated

that a host of properties depend on the size of the nanoparticles. The size (less than 6 nm) of the nanoparticles can be compatible with the thickness of the electron depletion layer, resulting in neck- or grain-controlled gas sensing action and hence enhanced sensitivity.

**46. Characteristics of Bonding Structures in Diamond-like Nanocomposite Film Deposited by RF-PECVD Technique at different Argon gas ambience**

**S. Das, S. Jana, P. Ghosh and U. Gangopadhyay**

Meghnad Saha Institute of Technology,
Kolkata–700 150
*E-mail : utpal_ganguly@yahoo.com*

Diamond–like Nanocomposite (DLN) films synthesized by the plasma decomposition of siloxane precursors have been considered for many industrial applications because DLN films are easier to produce than diamond films while exhibiting excellent physical and chemical properties close to those of diamond.

The film comprises of two amorphous interpenetrating network structures : one is "diamond-like" (a-C : H) network and the other is "glass like" (a-Si : O) network in an adjustable proportion. The "diamond-like" network forms the matrix whereas the "glass like" network forms the reinforcements of a typical nanocomposite structure and, therefore, the name DLN. The presence of a-Si : O network as a reinforcement matrix distinguishes the DLN film from conventional DLC film. The material possesses a number of unique bulk and surface properties like hardness with flexibility, good thermal stability, greater corrosion and wear resistance etc. Moreover, the interpenetrating networks are mutually stabilized by chemical bonding that lead to low residual stresses.

The aim of this study is to get an optimum mechanical property of DLN films by controlling the residual stresses in the DLN films deposited by the RF-PECVD method. Diamond-like nanocomposite (DLN) films are deposited on glass substrate using a radio frequency plasma-enhanced chemical vapor deposition (rf-PECVD) system and their structural bonding characteristics and mechanical properties are investigated as a function of the carrier gas (Argon) and the load power. It is found with the deposition of DLN films at different conditions that the sp3/sp2 ratio of carbon in the films and the hardness of the films increased up to a certain concentration of Argon gas flow and load power value.

**47. Synthesis and characterization of Silver (Ag) nanowires by solution phase route for Electronics applications**

**Salaimutharasan. G[1], Mohamed Javid. M[1], Siva. C[1], Prabaharan. M[2] and Ashok. K[1]**

[1]Department of Physics and Nanotechnology,
SRM University, Kattankulathur, Chennai
[2]Department of Chemistry, SRM University,
Kattankulathur, Chennai

Nano-sized ZnO and $Zn_2SnO_4$ (Transparent Conducting Oxide) have been synthesized using Sol gel synthesis method. The synthetic conditions and the calcination behaviors of nano sized ZnO and $Zn_2SnO_4$ have been studied. The crystallinity and particle size of the prepared metal oxides of ZnO and $Zn_2SnO_4$ have been characterized with X-Ray diffraction (XRD) spectroscopy and Atomic force microscopy(AFM). The morphology information of a synthesized samples have been analyzed with Scanning Electron Microcopy(SEM) to find the average grain size of 42 nm of binary and ternary metal oxides.

**48. Deriving Electricity through Waste ϑ-Radiations**

**Abhishek Sharma[#] and Pratyush Deyasi[*]**

[#]Electrical Engineering Department,
[*]Information & Technology Engineering Department,
Rungta College of Engineering & Technology,
Chhattisgarh Swami Vivekanand Technical University,
Rungta Educational Campus,
Khoka Road, Kurud, Bhilai (C.G.)–491 024, India
*E-mail : [#]abhishek1987sharma@gmail.com, [*]pdeyasi@rediff.com*

Proved by space studies, CNT's are resistant to most of radiations. So they can provide a base where ã radiations, from nuclear reactor waste Cd rods can be converted into the required energy form. For this, an inner hollow with Au coated Pb cylinder having CNT's (Au tipped) and uniform magnetic field. The Xe atoms ionized due to ã radiations, flow through nanotubes, absorbing ð-bonded electrons. This results into formation of potential difference and production of electricity (DC). By using this process we would be able to use up ã -rays in an environment friendlier means and also are able to solve the disposal problem of ã-radiative Cd/Control rods.

# 98<sup>th</sup> Indian Science Congress

**January 3-7, 2011, Chennai**

# VI

# LIST OF

# PAST SECTIONAL PRESIDENTS

# PAST SECTIONAL PRESIDENTS

## Section of Materials Science

1.  P. V. S. Rao — 1991
2.  V. Rajaraman — 1992
3.  R. K. Datta — 1993
4.  Devadatta Sinha — 1994
5.  Baldev Raj — 1995
6.  K. J. Rao — 1996
7.  C. Ganguly — 1997
8.  S. K. Pabi — 1998
9.  S. S. Agarwal — 1999
10. D. N. Bose — 2000
11. A. K. Barua — 2001
12. H. S. Maiti — 2002
13. Suresh Chandra — 2003
14. K. A. Padmanabhan — 2004
15. Neeraj Khare — 2005
16. R. K. Pandey — 2006
17. R. C. Agarwal — 2007
18. S. N. Sahu — 2008
19. Karnati Somaiah — 2009
20. I. Manna — 2010